USING UAS IMAGES TO REMOTELY ESTIMATE SOIL MOISTURE CONTENT IN THE RED RIVER VALLEY

A Thesis
Submitted to the Graduate Faculty
of the
North Dakota State University
of Agriculture and Applied Science

By

Talon Clancy Mack

In Partial Fulfillment of the Requirements
for the Degree of
MASTER OF SCIENCE

Major Program:
Agricultural and Biosystems Engineering

April 2021

Fargo, North Dakota

North Dakota State University
Graduate School

Title

USING UAS IMAGES TO REMOTELY ESTIMATE SOIL MOISTURE CONTENT IN THE RED RIVER VALLEY

By

Talon Clancy Mack

The Supervisory Committee certifies that this ***disquisition*** complies with North Dakota State University's regulations and meets the accepted standards for the degree of

MASTER OF SCIENCE

SUPERVISORY COMMITTEE:

Xinhua Jia
Chair

J. Paulo Flores

Stephanie Day

Xin Sun

Approved:

7/8/2021
Date

Kenneth Hellevang
Department Chair

ABSTRACT

Accurate measurements of soil moisture in a timely manner are necessary in making critical management decisions, but it is often very difficult to obtain. Even though soil moisture can be measured on the ground using various methods, or estimated via satellite imagery, soil moisture conditions at a field scale can be more beneficial. Since Unmanned Aircraft System (UAS) technology has become an effective tool in many different ways for producers and researchers, the spatial and temporal gaps between the ground and the satellite approaches can be fulfilled with the use of UAS. In this study, multi-spectral images were collected over an agricultural field in the Red River Valley from an UAS platform. Using this data, the soil moisture content was calculated, and a soil moisture map was developed. The remotely sensed soil moisture was then compared to the in-situ field moisture measurements to gage the soil moisture mapping accuracy.

ACKNOWLEDGMENTS

I would like to first thank my committee chair, Dr. Jia for her continuous support and providing the resources for me to make it through graduate school, my other committee members, Dr. Flores, Dr. Day, and Dr. Sun for their knowledge and support, and Dr. Jia's research team, Dongqing Lin, Kristen Almen, Uday Vaddevolu, Minglian Lin, and Shad Mack for all their assistance with the project. I would also like to thank my family and friends for their support in my continued education, and most importantly my fiancé Sam for putting up with all the late nights and long hours. Lastly, I would also like to thank my canine partners, Louie and Whiskey for helping in the field from time to time and keeping me company through the many hours of writing.

DEDICATION

I would like to dedicate this thesis to a major influence in my education, my grandfather Laurel Thoreson who held a master's degree in education and encouraged to me to continue school and obtain a master's degree.

TABLE OF CONTENTS

LIST OF TABLES

LIST OF FIGURES

LIST OF ABBREVIATIONS

ac .....Acres

avg.....Average

°C .....Degrees Celsius

cm.....Centimeters

K.....Degrees Kelvin

g.....Grams

GPS .....Global Positioning System

Ha.....Hectares

NASA.....National Aeronautics and Space Administration

NDVI.....Normalized Difference Vegetation Index

NIR.....Near Infrared

nm .....nanometers

RGB .....Red Green Blue

RRV .....Red River Valley

RTK.....Real Time Kinematic

SM.....Soil Moisture

SMAP.....Soil Moisture Active and Passive

TDR.....Time Domain Reflectometry

TVDI .....Temperature Vegetation Dryness Index

UAS.....Unmanned Aerial System

UAV .....Unmanned Aerial Vehicle

µm .....Micrometers

LIST OF SYMBOLS

θ_m .....Mass water content

θ_v .....Volumetric water content

ρ_d .....Bulk density of soil

ρ_w .....Density of water

ρ_{NIR} .....NIR reflectance values

ρ_{red} .....Red reflectance values

γ .....Slope

λ.....Wavelength in nm

b.....y intercept

M .....Slope of soil line

T_s .....Surface temperature

T_{smin} .....Minimum surface temperature

M_s .....Mass of dry soil

M_w .....Mass of water evaporated in oven

V_{total} .....Volume total

V_w .....Volume of water

1. INTRODUCTION

1.1. Background

In the Red River Valley (RRV), rainfall and snowmelt are the main water source for agriculture. Knowing the soil moisture in the field and obtaining it in a timely manner can be beneficial to the growers in the RRV. It helps growers make timely decisions on planting, crop variety selection, fertilizing, chemical applications, tillage operations, and harvesting. Good decisions on the management practices have the potential to maximize crop yields and minimize operation costs. Higher soil moisture in the field can lead to different costly complications, such as equipment becoming stuck in wet spots, which can halt production, higher fuel usage, large soil disturbances, lower machine efficiency, and equipment break downs. Planting, emergence, and early growth for a crop are highly dependent on the soil moisture conditions. Drought or waterlogging can both cause crop yield decreases.

During the springtime, after snowmelt, when the soil moisture conditions are in favor of crop germination, there is a narrow time window that producers have to plant their crops. However, most times in the RRV, many farm fields have numerous wet areas, or the entire field may be too wet for field operations. In these wet areas, it may be beneficial to use an alternative variety that is more tolerant to waterlogging conditions to minimize impacts on crop yield. Monitoring the soil moisture status right after planting can also be beneficial for different reasons. The performance of the farm equipment is affected by the soil moisture because wet soils can lower machine performance in the field and raise fuel costs. Water management strategies, irrigation, or drainage are also dependent on the soil moisture content of the field to achieve a higher crop yield potential.

In the fall, producers need to know the soil moisture conditions in the field in order to determine the time and equipment types for harvesting. Wet falls can lead to delayed harvest, while dry falls can result in early harvest to avoid yield losses. There may be specific areas in a field that should be avoided due to excessive soil moisture and soil type. In some cases, producers also may need to purchase specialized equipment for higher soil moisture field conditions. Without knowing the soil moisture conditions at a field scale, one cannot determine when and how to perform field operations.

"Precision agriculture is economically and ecologically promising and it will one day be standard practice" (Santhosh, 2003). In today's farming, Unmanned Aerial Vehicles (UAVs) are increasingly used to provide various timely measurements at field scales, such as fertilization recommendation, crop yield estimates, plant status monitoring, crop disease monitoring, insects diagnosis, contour mapping, water management, etc. Farming smarter with UAVs may become the key to increase yields and limit costs. Using UAV images to estimate the soil moisture can be one of the benefits to help farmers make a timely decision in farming practices.

1.2. Objectives

The main objectives of this study were:

(1) To determine data processing protocols and to develop soil moisture maps at a field scale using UAS collected imagery;

(2) To compare the remotely sensed soil moisture data with in-situ measured soil moisture data; and

(3) To create a soil moisture map protocol that others can follow and develop soil moisture maps for fields based on the imagery and backed up via in-situ data.

The objectives were completed by first collecting field data, which included in-situ soil moisture measurements and UAS flights, second processing the collected data into a useful form, and finally producing a soil moisture map of the flighting area.

2. LITERATURE REVIEW

2.1. Soil Moisture

"Soil moisture is an environmental descriptor that integrates much of the land surface hydrology and is the interface between the solid earth surface and the atmosphere" (Engman, 2000). The definition of soil moisture content or the surface soil moisture, is the amount of volumetric water content in a thin soil layer close to the surface (Leng, 2018). Soil moisture control is essential for the high value crops in the RRV. Soil moisture determination benefits more than just agriculture, it also serves as an important factor in flood predictions, especially in the RRV where flooding is a common occurrence. Soil moisture in the fall can play an important role and influence the severity of flooding in the following spring. Since a drier soil can store more snowmelt water than a wetter one, the drier soil can absorb more water, reducing runoff and flooding (Lakshmi, 2017).

2.2. Factors Affecting Soil Moisture

2.2.1. Mechanical Composition

A soil's texture as defined by (Hillel, 1998) is the classification of soil based on the particle size or the division of soil into sand, silt, and clay according to particle size. Mechanical composition or the soil texture is the amount of each of these classes in a soil. According to the percentage of sand, silt and clay in a soil, soils are classified into different soil types. Finer soil texture like the clayey soils in the RRV retain more water than sandy soils due to more surface area for water. In general, the smaller the particle size, the higher the water holding capacity.

2.2.2. Crop Residue

Residue is the material left by a crop after harvest. Depending on where the crop residue is located, it can affect the water movement into the soil, and the soil moisture and temperature

of the soil under it. Residue that is open to the surface aids in water movement while buried residue restricts water movement. A high amount of crop residue on the surface can possibly trap moisture or insulate the ground to an extent potentially decreasing evapotranspiration.

2.2.3. Topography

Topography according to the dictionary is the "configuration of a surface including its relief and the position of its natural and man-made features" (Merriam-Webster, 2019). Highly varying topography with high slope areas tend to promote runoff due to the tendency of water to travel in the direction of least resistance. Flat areas have less potential, allowing water to pond and slowly infiltrate or evaporate depending on soil conditions and composition. Topography can also affect the energy input from the sun to the soil. This can increase or decrease the rate of evapotranspiration from the soil and crop.

2.3. Soil Moisture Measurement Methods

Soil moisture content is described as a ratio of the mass of water to the mass of dry soil or volume of water to the total volume of the soil. The volume-based soil moisture content can be estimated from the mass-based water content and the soil bulk density.

There are several common methods used for soil moisture measurements. The direct and standard method is the gravimetric method. Most methods are indirect, and do not measure soil moisture directly. Indirect methods measure a property of the soil using a soil moisture sensor that can be related to the soil moisture rather than the soil moisture itself (Evans, 1996). Some common indirect methods are tensiometers, electrical resistance, and neutron scattering. Common conventional measurements are costly and only provide the information at collection points (Pietroniro, 2005). These details are discussed below.

2.3.1. Feel

This is a common method used by experienced growers and scientists. Soil is worked with the fingers to form a ribbon and from the structure one guesses the relative moisture. It is an easy method to implement but it is generally unreliable (Evans, 1996).

2.3.2. Gravimetric

Gravimetric, which can also be called thermos-gravimetric technique, is commonly used and has been employed by many as the standard reference for determining soil moisture content (Lekshmi, 2014). This is a direct method that is conducted in a laboratory. The first step is to collect undisturbed soil cores from the field. The next is taking the samples to the laboratory, weigh the samples, and dry them for at least 24 hours at 105 °C depending on sample sizes. After drying, the soil is weighed again. Compared to the original wet soil sample, the soil moisture content can be calculated from the moisture difference and the total volume of the soil core. The following equation shows how the soil water content is calculated:

$$\theta_m = \frac{M_w}{M_s} \quad (1)$$

where:

θ_m = Mass water content (g/g)

M_w = Mass of water evaporated in oven (g)

M_s = Mass of dry soil (g)

Most methods for soil moisture estimates are for volume-based moisture content, which is:

$$\theta_v = \frac{V_w}{V_{total}} \quad (2)$$

where:

θ_v = Volumetric water content (cm^3/cm^3)

V_w = Volume of water (cm^3)

V_{total} = Volume total (cm^3)

The relationship between the two soil moistures is estimated from:

$$\theta_v = \frac{V_w \rho_d}{\rho_w} \quad (3)$$

where:

ρ_d = bulk density of soil (g/cm^3)

ρ_w = density of water (g/cm^3)

2.3.3. Electrical Resistance

This method usually uses two electrical probes and a block commonly made of gypsum, but other materials can include nylon or fiberglass. The soil moisture is calculated based on the resistance of the electrode in the block that is in equilibrium with the surrounding soil. This can be a limited method depending on soil type and moisture range (Hillel, 1998), as well as soil salinity.

2.3.4. Tensiometer

Tensiometers have porous ceramic tips connected to vacuum tight tubes and gages that measures the amount of suction or soil matric potential. The porous tip is first completely soaked in water and then buried in the soil. The tip and the soil reach an equilibrium, where the soil draws moisture out of the tip, causing a drop in hydrostatic pressure. This measures the matric potential of the soil and gives the user an idea of the soil moisture based on soil water retention curve. The main disadvantage of using a tensiometer is the measurement range. They tend to only work from zero to 1 atm (1 bar), which works well for moist soils, but does not work for the dryer soils (Hillel, 1998).

2.3.5. Neutron Scattering

Neutron probes use radiation to detect soil moisture. The measuring of fast neutrons released vs slow neutrons that return is how the method works (Hillel, 1998). These probes tend to be versatile and quick, but due to the radioactive component, they have heavy restrictions on handling, shipping, and transporting (Lekshmi, 2014). They are also limited to point measurements.

2.3.6. Time Domain Reflectometer

This method has become widely used and adapted as a mode of measuring soil moisture at a quick rate. Solid rods or probes are stuck in the ground with cables connecting to a device that sends and receives pulses. The soil moisture is determined from sending a pulse through the probes and measuring the time it travels to the end of the probe and back to the sensor (Hillel, 1998).

2.4. Satellite Mapping

Remote sensing from satellite is widely researched for a multitude of systems. SMAP (soil moisture active and passive) is being studied in great lengths around the world. NASA developed SMAP, which makes direct observations of soil moisture and the freezing or thawing of the land from space (Entekhabi, et al., 2010). These satellite images and continued research are quite beneficial to the globe. Using satellite, land most places in the world can be observed and analyzed with large swaths. This is extremely beneficial for looking at regions as a whole. The technology is rapidly growing with more complex algorithms and synergy combinations of sensors. Table 1 summarized from Peitroniro et al. (2005) shows some of the advantages and disadvantages of different remote sensors used by satellites that have been used to estimate soil moisture.

Table 1. Summary of remote sensing methods for soil moisture.

Wavelength	Property	Advantages	Disadvantages	Sources of Error
Reflected visible and infrared (0.3 to 3.0 μm)	Reflectance	High resolution	Cloud cover limits No direct relationship between reflectance and soil moisture	Vegetative cover Surface roughness Atmosphere
Thermal infrared (10 to 12 μm)	Temperature	High resolution Large swath Soil texture insignificant	Bare soil only Cloud cover limits	Vegetation Topography Atmosphere
Active microwave (1-100 cm)	Backscatter coefficient	All-weather High resolution Vegetation penetration	Noisy data stream Complex interaction with surface	Roughness Vegetation Topography
Passive microwave (1-100 cm)	Microwave emission (brightness temperature)	Nearly all-weather Large area coverage Vegetation penetration	Poor spatial resolution	Surface roughness Soil temperature Vegetative cover Atmosphere

Data from (Pietroniro, Toyra, Leconte, & Kite, 2005)

Landsat was first launched in 1972 and was the first satellite system to focus on the land surface as its main function. A study done by Rijal et al. (2012) used Landsat data to measure soil moisture at 15 cm depths in the RRV. This study did have limitations, the range of soil moisture measurement was between 0.20 and 0.40 cm^3/cm^3, though these are typical soil moisture values under average conditions.

One of the biggest issues with satellite data is the time that it takes to collect ground data to calibrate the remote sensing images to refine the algorithms. In relative aspect, the in-situ measurements provided point measurements, which were small data points compared to the area of the satellite's coverage. A satellite's resolution consists of square kilometer sized pixels because of the vast amount of land covered. This resolution would not be adequate at the field level because of the differences that can be present from one field to another in the same section or even from one end of the field to another. Using manned airplanes can help fill the gap

between the satellite remote sensing and the field measurements, but this tends to be expensive due to the costs associated with operating manned aircraft. This is where the UAS and its rapidly expanding market are proving to help and reduce costs of manned aircraft.

2.5. UAS

UAV is defined as an unmanned aerial vehicle meaning it can be any sort of vehicle that is controlled remotely in the air. UAVs are also referred to as drones or UAS (unmanned aircraft system). When describing more than just the UAV itself and including the payload and remote control system, the term UAS is used. There are two main types of UAS, fixed wing and multi-rotor. Both of these have their advantages and disadvantages. Multi-rotor UAS have the advantages of maneuverability, hovering, and ease of use, but they lack in endurance. Fixed wing UAS have the ability to cover large areas of land and have a longer flight time, but they are harder to control manually or are unable to be controlled manually and lack the ability to maneuver in congested areas.

As UAS and sensors become more readily available, so do their uses. A statistical study done by Hassen-Esfahani et al. (2017) showed the advantages to using UAS to fill the spatial temporal scale gap. The spatial gap is one of the biggest downsides with satellite data when it comes to defending data and looking for more “field level” results. In a resolution aspect, the point system common with in situ measurements that are used, make for small data points compared to the large spatial resolution of satellites that may be unable to differ fields in the same section. Using small UAS to help back up and confirm data being recorded by satellites or larger aircraft is extremely beneficial to the better development of technology and imagery. Satellites, although fairly reliable, can struggle to collect usable data with bad or cloudy weather. Due to specific timing of the data collection because of a satellite’s path, a data set can be missed

in a desired timeframe. Conversely UAS are ready whenever the user is ready to collect data at optimal times.

2.6. Sensors for Remote Measurements

2.6.1. Microwave Sensors

Microwave sensors are widely used sensors for remote sensing of soil moisture (Ma, 2019). Most commonly, the microwave sensors can be used on satellites, but also can be mounted to manned aircraft, though these sensors are large and expensive to use. Recently, some microwave sensors have been adapted to a UAS platform, but they are still uncommon.

2.6.2. Multispectral Sensors

Multispectral sensors measure an array of different wave lengths in the electromagnetic spectrum, which can be used to detect different variations of the Earth's surface. Commonly a combination of the red, green, blue, near infrared, and infrared frequencies are used by multispectral sensors.

Anything that has a temperature above 0 K emits electromagnetic radiation (Kuenzer, 2013). In the electromagnetic spectrum, the majority of thermal radiation is located in the infrared portion that is invisible to the naked eye. Thermal radiation is located in the visible range when temperatures are high enough, such as when metal becomes "red hot" in color when heated. Thermal infrared sensors have been used on satellite platforms for decades. Sensors continue to become more advanced and when used in synergy relationships with other sensor with different wavelengths such as microwaves, the output data becomes even more useful. Kuenzer et al. (2013) describes how there is not an obvious relationship between thermal infrared and soil moisture, but evapotranspiration, specific heat capacity, and emissivity is

related to the water content of the soil. Studies use this information to form an indirect relationship to determine soil moisture.

One of the popular methods of determining soil moisture using multispectral sensors is the temperature-vegetation dryness index (TVDI) shown in the following equation from Sandholt et al. (2001). The basis of this method starts with the normalized difference vegetation index (NDVI) and surface temperature (T_s) that is taken from remote sensing measurements and plotted to form Figure 1. Figure 2 shows more details of the TVDI triangle.

$$TVDI = \frac{T_s - T_{s_{min}}}{a + b * NDVI - {}_{s_{min}}} \quad (4)$$

where:

NDVI = normalized difference vegetation index

T_s = remotely sensed soil temperature °C

T_{smin} = minimum surface temperature in the triangle °C

a and b = parameters defining the dry edge modelled as a linear fit to T_{smax} = a + b*NDVI

and T_{smax} = maximum surface temperature observed °C

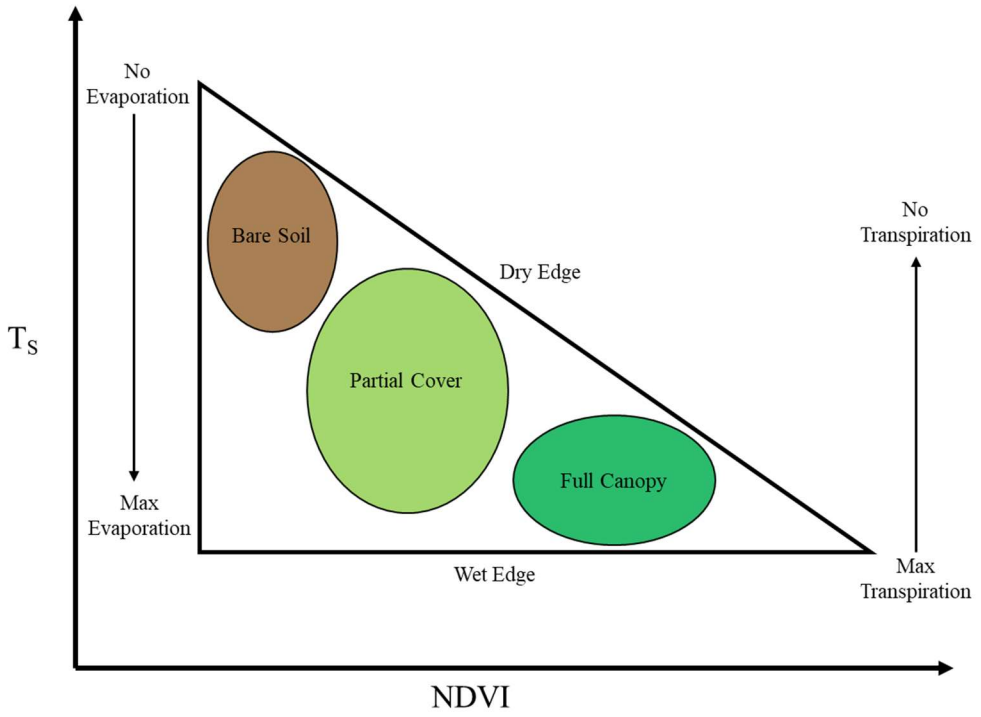

Figure 1. T_s/NDVI Triangle (Lambin, 1996) showing how the triangle method is used.

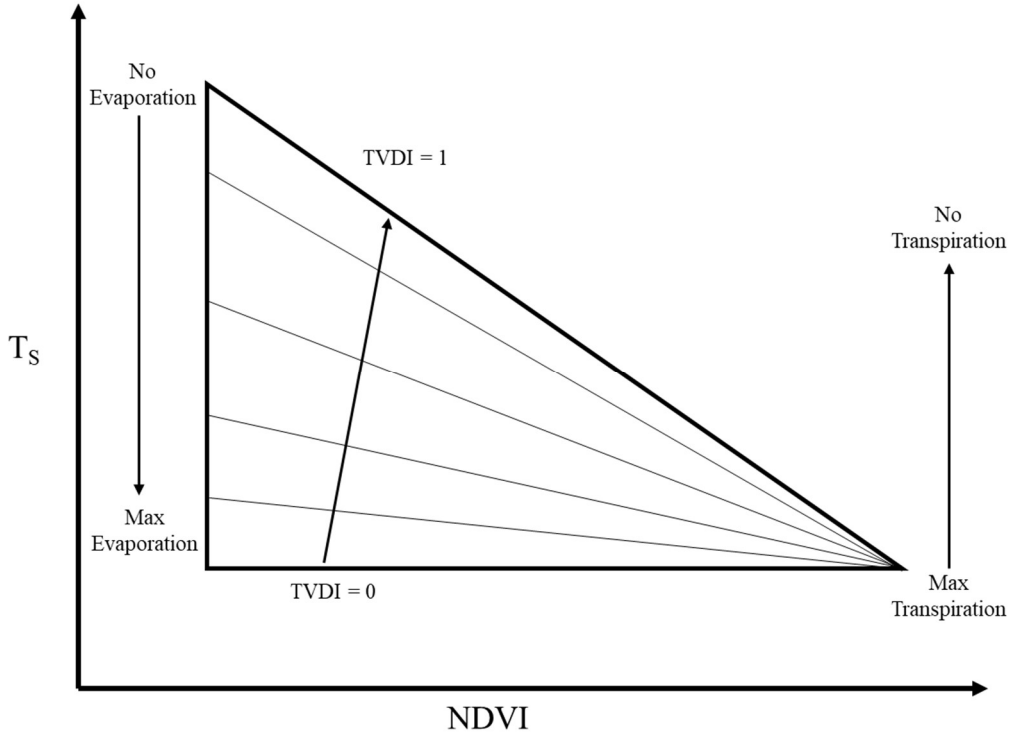

Figure 2. Picture illustration of TVDI (Sandholt, 2001).

Figure 2 is a modified version of Figure 1 that expresses how different values of TVDI fall into the NDVI vs T_s triangle relationship. From this point, Sandholt et al. (2001) used a scatter plot of simulated root zone soil moisture vs TVDI to form a linear relationship between the TVDI and the soil moisture. This showed that lower TVDI values related to higher soil moisture values.

Once TVDI values are assigned from the NDVI and T_s map data, the linear relationship from surface soil moisture content is used to map the soil moisture, while volumetric water content requires in-situ soil core measurements (Wigmore et al., 2019).

Another method by Chang and Hsu (2018) used a linear equation derived from the near-infrared and red wavelengths. The equation they calculated is as follows:

$$SM = \frac{\frac{\lambda_{red}}{\lambda_{NIR}+0.015}-0.08}{\sqrt{1+\frac{1}{0.015^2}}} \quad (5)$$

where:

SM = Soil moisture (0 to 1)

λ = Wavelength in nm

The data was entered into ArcGIS raster calculator to obtain the surface soil moisture at determined points on the map that were compared to manual measurements. Chang and Hsu (2018) found that their linear equation was more accurate to the in-situ measurements than by the TVDI method.

Another study used a combination of red and near infrared wavelengths in a scatter plot collected using a multispectral sensor (Amani et al, 2017). Using the multispectral data collected, a soil line is formed on the bottom edge of the scatter plot using the equation:

$$\rho_{NIR} = \gamma\rho_{red} + b \quad (6)$$

where:

ρ_{NIR} = NIR reflectance values (µm)

ρ_{red} = red reflectance values (µm)

γ = slope

b = intercept

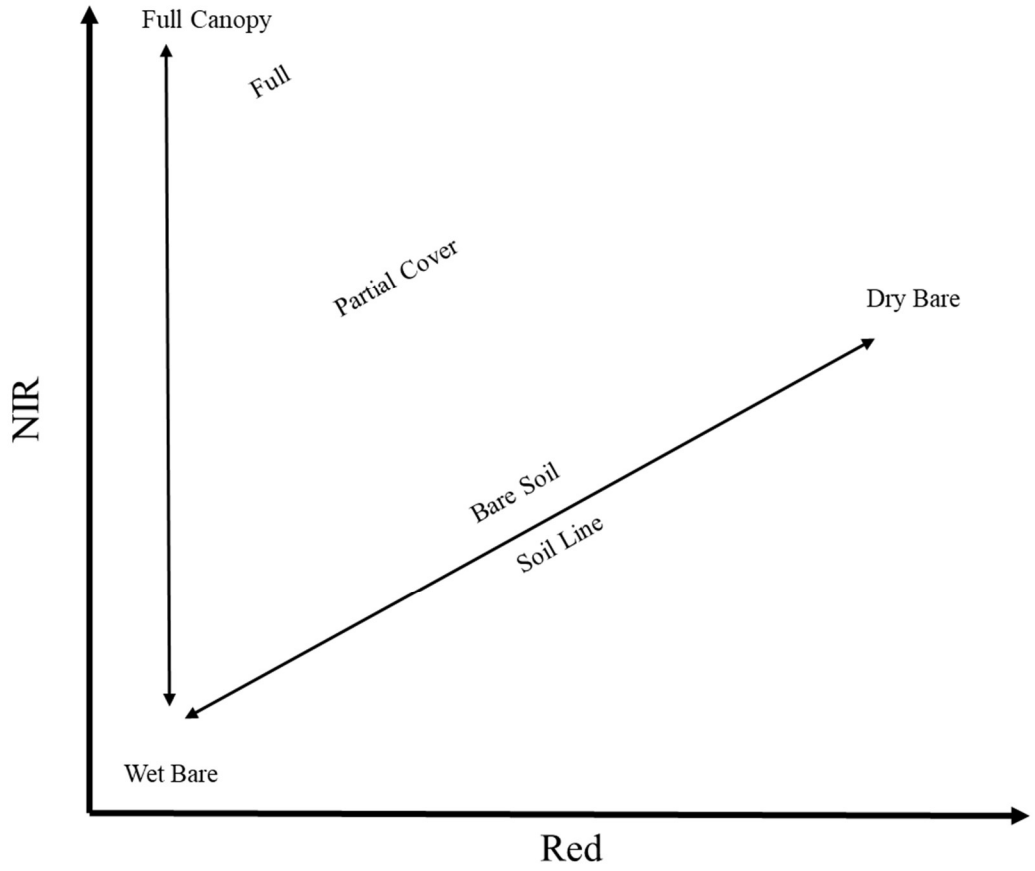

Figure 3. NIR vs red soil line (Amani et al., 2017).

Figure 3 made from Amani et al. (2017) shows how pixels fall in the Red vs NIR space with the wettest and barest pixels near the origin, the coverage changing in the Y direction, and the soil moisture changing in the X direction. Using this equation, Amani et al. (2017) estimated the soil moisture (SM) of the points from Landsat 8 data. The following equation represents the SM values in the figure:

$$SM = \frac{\rho_{NIR} + \frac{\rho_{red}}{M} - b}{\sqrt{1 + \frac{1}{M^2}}} \quad (7)$$

where:

ρ_{NIR} = NIR reflectance values (µm)

ρ_{red} = red reflectance values (µm)

M = slope of soil line

b = intercept of perpendicular line indicating wet and bare point of soil line

2.6.3. Thermal Remote Sensing

Thermal remote sensing sensors on UAS have gained popularity with more affordable options. A study done by Quebajo et al. (2018) used thermal imagery from a UAS mounted sensor to monitor sugar beet water stress. They used soil moisture sensors throughout the study but did not find a true relationship with the soil moisture. A relationship between the sugar content and the water stress was observed by the thermal imaging. A paper by Chang and Hsu (2018) used UAS with thermal sensors to detect soil moisture in the field and found a strong relationship, though more research is needed for better results.

3. METHODOLOGY

3.1. Study Site

The study site for this experiment was located in the RRV region just north of Moorhead, MN. The data collection took place in a 32 ha (80 ac) tile drained soybean and corn rotation field. The field was instrumented with a weather station, soil moisture sensors, observation wells, and an eddy covariance weather station (Kolars et al., 2019; Niaghi et al., 2019). Early in the data collection, the field was covered in high corn residue from the previous year due in part to a minimal tillage practice put in place. In the last data collection, soybeans are visible and have an established canopy. Figure 4 shows the location of the study site.

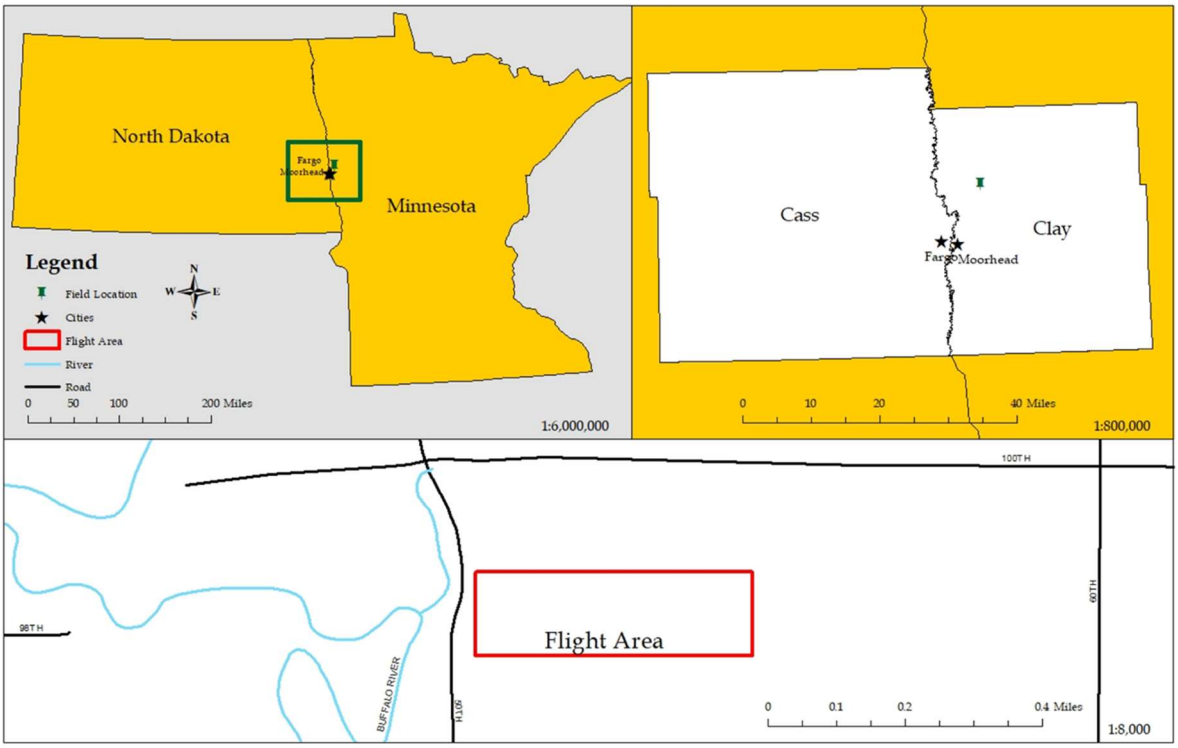

Figure 4. Field location.

The field contains a tile drainage system that runs from east to west and has a spacing of 12.2 m. A system of gates is used to maintain the water level in the field. This tile drainage system is doubled as a subirrigation system as well for dry weather, taking water from the nearby

stream and pumping it in the tile system from the high side in the east side of the field (Kolars et al., 2019).

The data collection area itself consisted of 17 ha rectangle in the center of the field. This area was used to minimize the field edge effect and centralize the field's weather station in the middle of the data collection area.

The soil type of the field is consistent of the RRV, clay and silt make up the majority of the soil for the field. The dominate soil in the field is a Colvin silty clay loam with Overly silty clay loam and Bearden silt loam roughly splitting the remaining area. Due to the high clay and silt content, the water drainage rate is slow, as is typical in the RRV. The map in Figure 5 shows the entire field and soil types in it according to Web Soil Survey.

Figure 5. I376A is a Colvin silty clay loam, I383A is an Overly silty clay loam, and I467A is a Bearden silt loam. Data taken from Web Soil Survey (USDA, 2018).

3.2. Equipment

3.2.1. UAS

For this experiment, a DJI Matrice 600 UAS was used to carry the sensor payload. This UAS is relatively common among the research and commercial sectors. It supports a number of sensors from DJI that can be used out of the box to collect remote sensing data. This particular DJI Matrice was adapted to carry two sensors at the same time. This modification was done at North Dakota State University in the Agricultural Engineering Department using the original sensor mount for the original DJI sensor and gimbal, and a custom 3D printed gimbal to accommodate and stabilize the second sensor. This setup of the UAS with sensors can be seen in Figure 6.

Figure 6. DJI Matric 600.

3.2.2. Sensors

There were two sensors used in this experiment: a Micasense Altum multispectral camera (Figure 7) and a DJI FLIR Zenmuse XT2 thermal camera (Figure 8). The Altum collects data in six different bands: Blue – 475 nm center with 32 nm bandwidth, Green – 560 nm center with 27 nm bandwidth, Red – 668 nm center with 16 nm bandwidth, Red Edge – 717 nm center with 12

nm bandwidth, Near Infrared – 842 nm center with 57 nm bandwidth, and Long Wave Infrared – 8-14 µm. The Zenmuse XT2 camera collects data in the range of 7.5-13.5 µm, which makes it within the Long Wave Infrared range from the Altum. The difference in these sensors comes to the resolution of the sensors, the Zenmuse provides a higher resolution with more pixels in a given area than the Altum.

Figure 7. Micasense Altum sensor and gimbal.

Figure 8. FLIR Zenmuse XT2 sensor.

3.2.3. TDR Sensor

To collect in situ soil moisture data for the experiment, a handheld Field Scout time domain reflectometer (TDR) sensor (Figure 9) was used. Two different size probes were used for the measurements at 7.6 cm (3 in) and 20 cm (8 in) depth. Due to a high clay content of the soil, the sensor was calibrated according to the manufacture specifications in the lab for better alignment prior to each field measurements.

Figure 9. TDR sensor.

3.3. Data Measurements

The data for the experiment was collected in two different stages, one remotely with the UAS and one by hand in a grid pattern around the weather station in the center of the field. The UAS collected its images first and then right after, in situ measurements were taken. These measurements were collected five times total in the summer of 2019 with four successful collection events.

3.3.1. UAS Collected Data

The DJI Matrice UAS collected data via the two equipped sensors, Micasense Altum and FLIR Zenmuse XT2. Before flying, the Micasense Altum was used to collect a calibrated image using the included white calibration panel. The picture was taken over the white calibration panel to adjust for the reflectance from the sun. This calibration image is used later in the processing program to calibrate the collected images. Figure 10 shows the collection of the calibration image for the Altum sensor.

Figure 10. Micasense Altum multispectral sensor calibration image collection.

Before the first flight, control points were placed throughout the collection area to aid in the data processing and stitching of the pictures. These were a collection of green and white buckets and black and whites rubber mats at fixed points. A mat can be seen in Figure 11. All flights used the same collection path and ground control points. There was a total of eight buckets in the field and two checkered rubber mats that remained in the collection sight

throughout the season. These ground control points were also marked by a RTK GPS with sub inch accuracy to ensure they were placed consistently in case they were ever disturbed.

Figure 11. Image of control point mat from imagery used as a ground control point.

Using the installed DJI software, the area of interest was mapped out on a tablet and the program determined the optimal travel path to collect the data by incorporating a uniform flight height and percent overlap. The area of interest for this project was determined by battery life while still encompassing the in-situ grid around the weather station.

After a flight was conducted, the large raw data set was stored on a memory card for processing at a later time. To process the data and stitch the data into one set, the software program Pix4 mapper was used. This step took a significant amount of time and computing power. The ending result produced a useful data set that could be used in other programs.

To refine the data into a usable soil moisture index map, ArcGIS Pro was used to take the data and form the initial red and NIR images. A grid tool was used to average pixel data into a uniform 3 x 3 meter grid. From the grid, tables were formed for both the Red and NIR data. R Statistics then was used to determine the soil line based on a linear regression from the data tables produced in ArcGIS Pro. Parameters from the R Statistics data were used in equation (7) to determine the SM average of each 3 x 3 meter grid square in the ArcGIS Pro map and form a

SM map of the field. Figure 12 shows the data processing procedures and Figure 13 shows the UAS flight path for the data collection.

Figure 12. UAS data processing flow chart.

Figure 13. UAS flight pattern. The arrows show an example of UAS path.

3.3.2. TDR Collected Data

In order to have in situ field measurements that would be repeatable, a grid around the weather station was marked with flags before the first flight to maintain sampling consistency. The grid was based on the location of the drain tiles in the field, marked with paired measurements, over the drain tile vs. in the middle between two drain tiles. It was predicted that

the soil moisture would be different at the two locations depending on the water drainage management modes. This resulted in 13 paired measurement points around the weather station, giving a total of 26 measurement points. There were an additional two points by an observation well in the western part of the flight area and two more points by an observation well in the eastern part of the collection area. These areas were also divided by over the tile and in the middle between the tiles. Figure 14 shows the 30 measurement points in the field in red dots and highlighted in yellow squares. The remaining GPS points highlighted in blue squares are control points for the UAS where the buckets and the mats were located to aid in data processing.

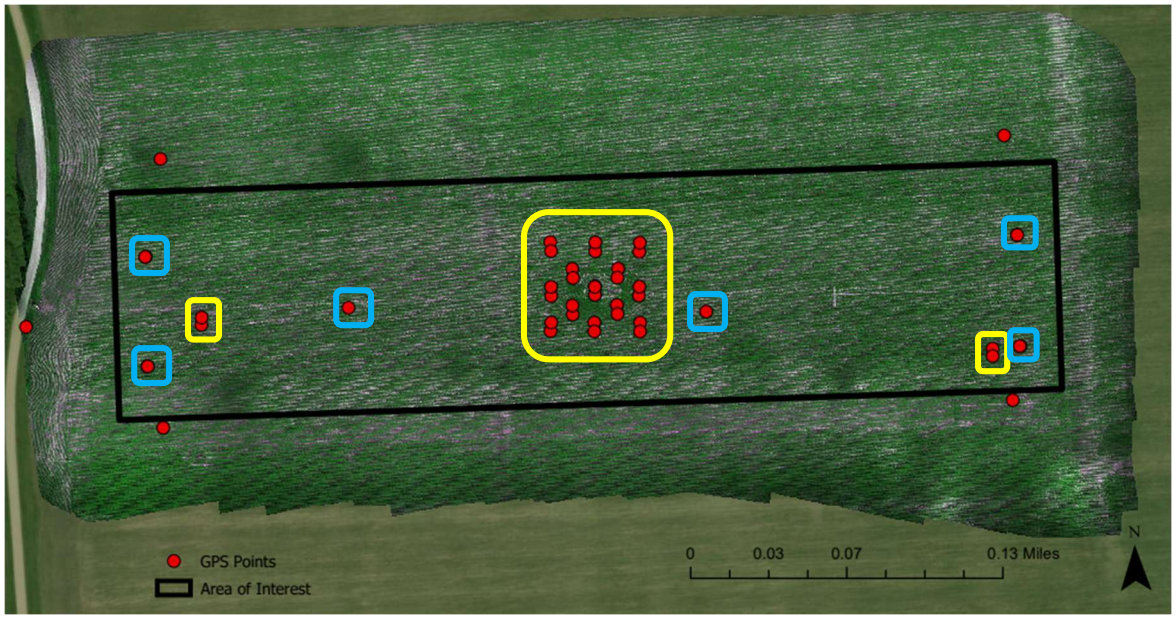

Figure 14. TDR soil moisture measurement points highlighted in yellow around weather station, control points highlighted in blue in the data collection area, and the black area outlining the study boundary.

Once the flight completed, all 30 points were measured for soil moisture with the TDR sensor using the 7.6 cm and 20 cm probes. The data was recorded and entered into a spread sheet for later comparison with the UAS data.

To calibrate the collected data by the TDR, soil samples from the field was packed into soil columns in the laboratory. These columns were packed to a bulk density of 1.25 g/cm^3 and

soil and water were mixed to preset the soil at soil moisture contents of 0%, 15%, 25%, 35%, 45%, and 53%. This data was used to create a calibration curve and form an equation to calibrate the field measurements by the TDR device. The TDR data collection method is shown in Figure 15.

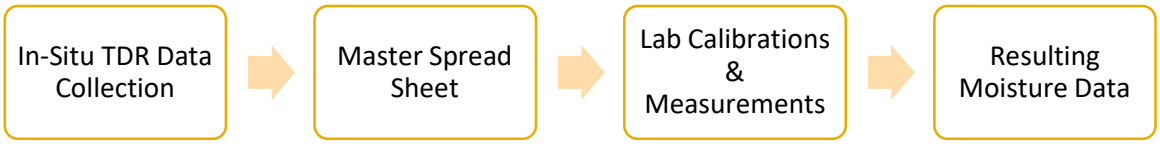

Figure 15. TDR data collecting flow chart.

4. RESULTS AND DISCUSSION

4.1. Data Sets

Four flights on May 7, May 14, May 23, and July 23, 2019 were post processed to develop soil moisture maps. Of the four flights, the three flights in May were collected over bare soil conditions. After the May 7th flight, the field was tilled in preparation for planting. The last flight took place on July 23, 2019 when the soybeans had grown significantly, providing crop cover throughout the collection site.

4.1.1. First Data Set Result

The May 7th data set was captured shortly after snow melt, leaving a significant amount of moisture. The vegetation condition was bare soil with corn crop residue. Soil temperatures were around 40 °F and the air temperature ranged from a low of 24 °F and high of 59 °F.

Due to the snow melt and some moisture events on the 1st, 2nd, and 3rd of May, this data set was found to have the second highest average red reflectance values and third highest average NIR reflectance values of the four data sets (Figures 16, 17, and 18). The average values were NIR = 0.264 and Red = 0.239. The high red reflectance values and lower NIR values placed it appropriately on the NIR vs Red triangle space. As seen on the NIR vs Red space in Figure 19, the data set had the highest average remotely sensed soil moisture content on the surface as shown in the SM content map. The remotely sensed average soil moisture content for this data set was 0.410, which is close to the soil field capacity value.

Figure 16. May 7, 2019 RGB image.

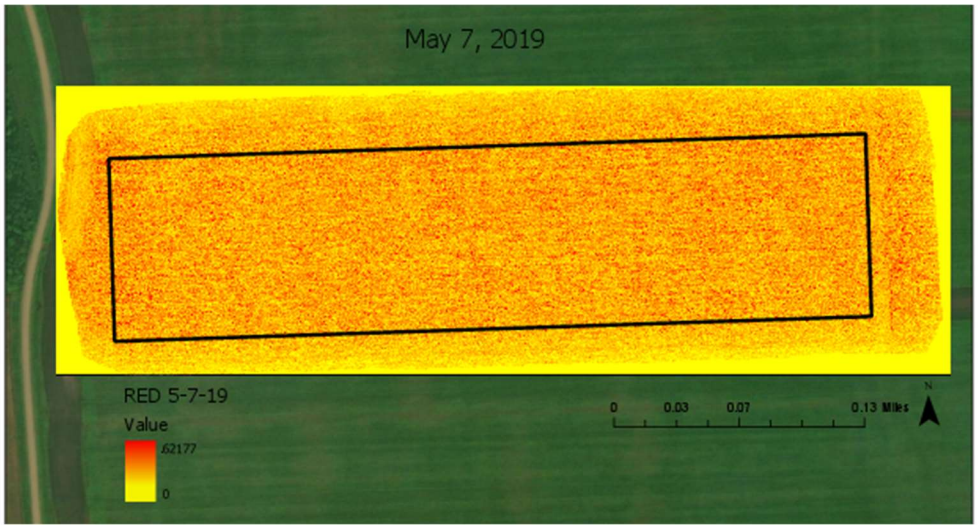

Figure 17. May 7, 2019 Red map.

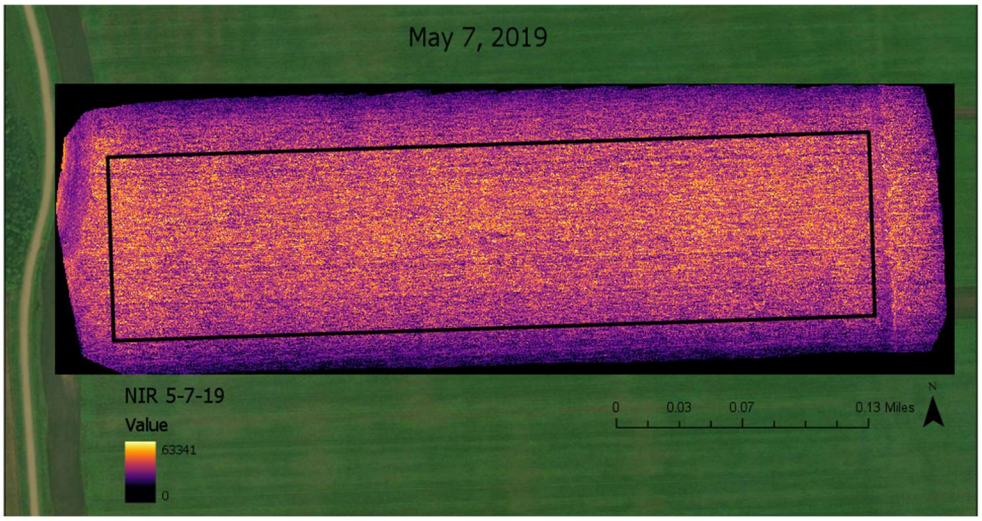

Figure 18. May 7, 2019 NIR map.

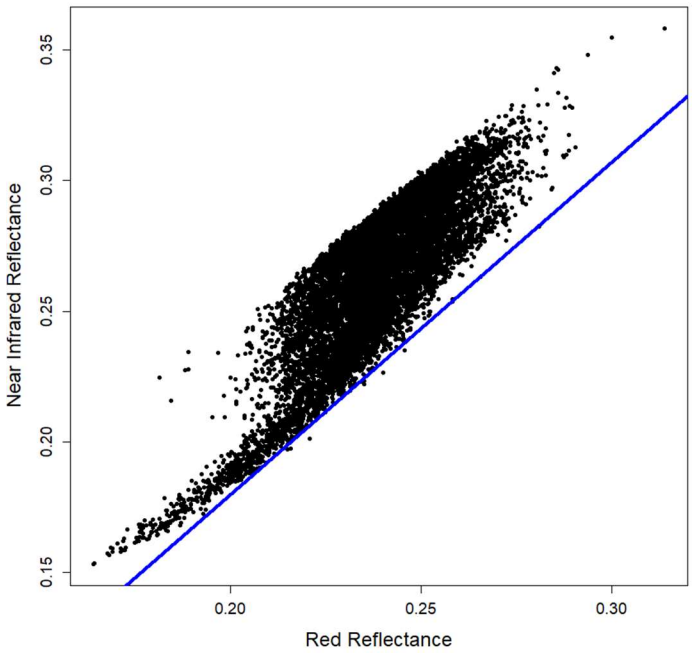

Figure 19. May 7, 2019 soil line graph.

4.1.2. Second Data Set Result

Between May 7th and May 14th there was little rainfall and there was also a tillage event recorded. The soil was bare and warmer than the previous flight as seen from the images (Figures 20, 21, and 22). Due to these circumstances, the NIR vs Red reflectance values followed the soil line tightly (Figure 23). The average NIR and Red reflectance values were low at: NIR = 0.161 and Red = 0.148. The remote soil moisture for this data set was also the driest at 0.155.

Figure 20. May 14, 2019 RGB image.

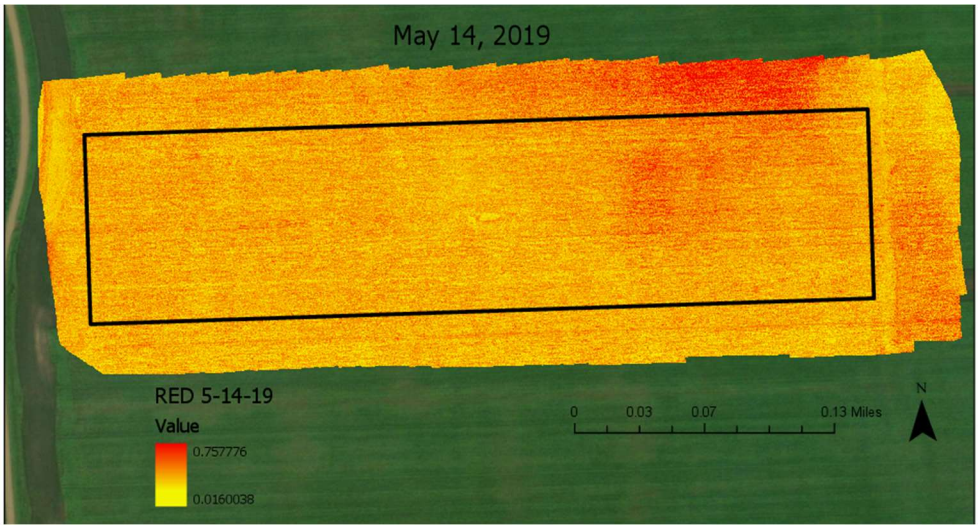

Figure 21. May 14, 2019 Red map.

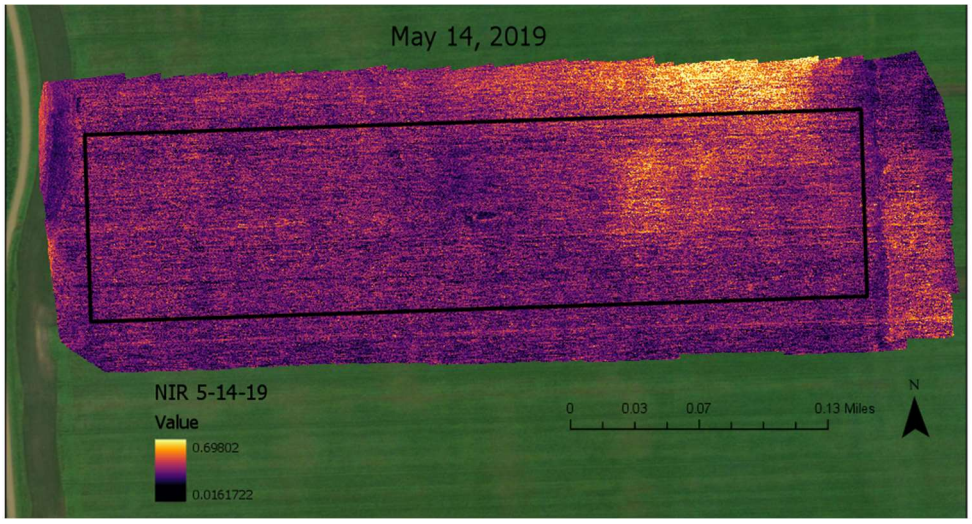

Figure 22. May 14, 2019 NIR map.

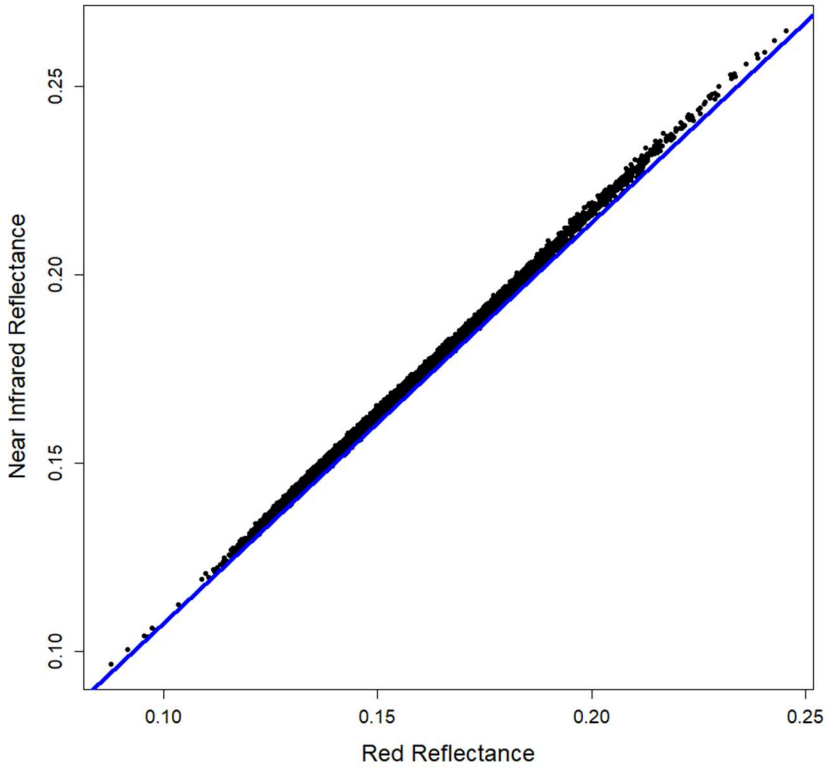

Figure 23. May 14, 2019 soil line graph.

4.1.3. Third Data Set Result

The May 23rd flight yielded the second highest remotely sensed soil moisture due to two significant rain events in the days prior (Figures 24, 25, and 26). On May 18th there was 0.68" of rainfall and on the 22nd of May, the day before the flight, there was 0.86" of rain. The NIR vs Red graph showed a similar pattern as May 7th (Figure 27). The average reflectance values were as follows: NIR = 0.284 and Red = 0.274. The average remotely sensed soil moisture was 0.397. This value was also similar to the May 7th flight.

Figure 24. May 23, 2019 RGB image.

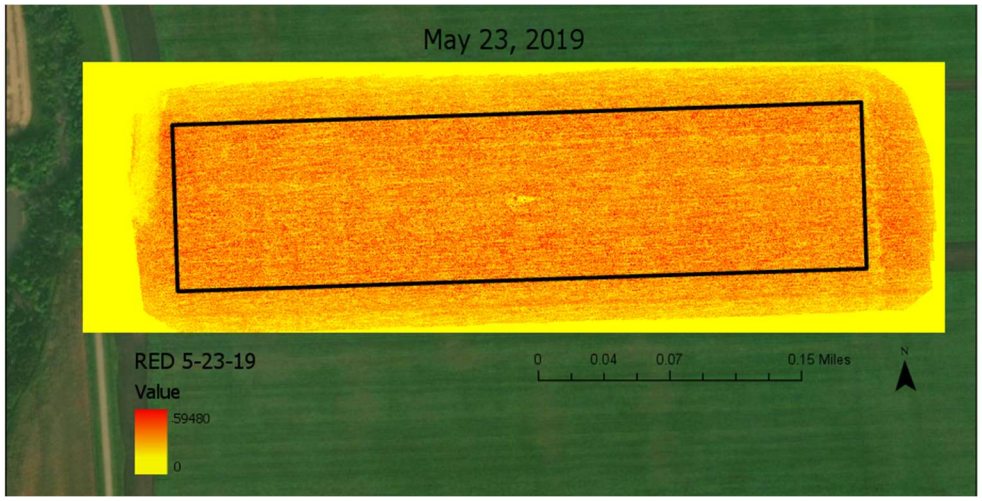

Figure 25. May 23, 2019 Red map.

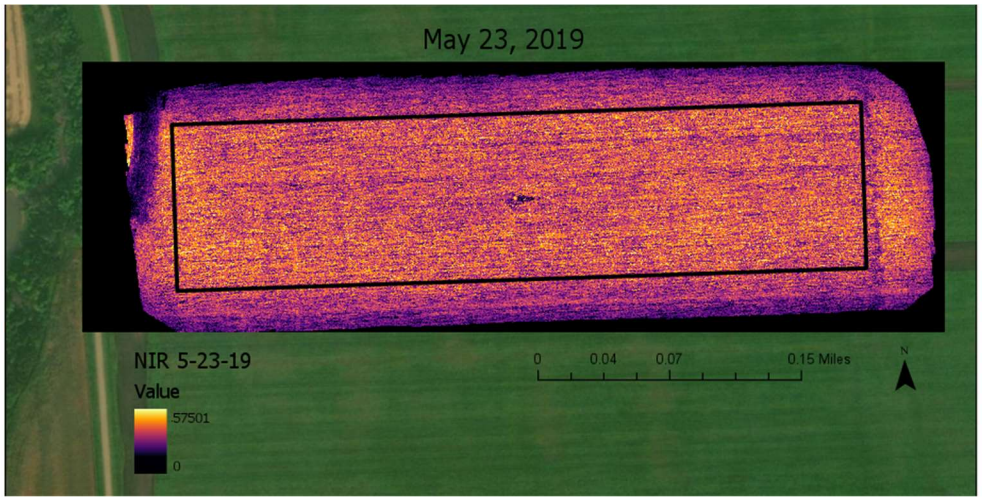

Figure 26. May 23, 2019 NIR map.

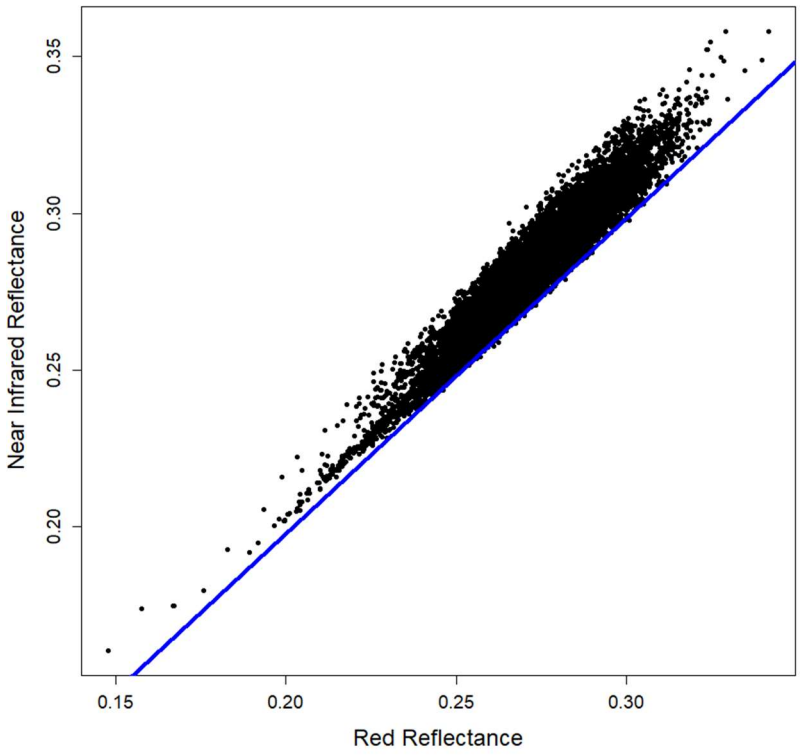

Figure 27. May 23, 2019 soil line graph.

4.1.4. Fourth Data Set Result

The last flight was carried out after the soybean crop had been well established. There were some rain events leading up to this date, but due to higher temperatures, growing crops, and an operational tile system, the remotely sensed soil moisture was low at 0.188. The images are shown in Figures 28, 29, and 30. The NIR vs Red graph showed the presence of vegetation with a high NIR value and dryer conditions with the lower Red value (Figure 31). The average NIR reflectance value was 0.283 and Red reflectance value was 0.176.

Figure 28. July 23, 2019 RGB image.

Figure 29. July 23, 2019 Red map.

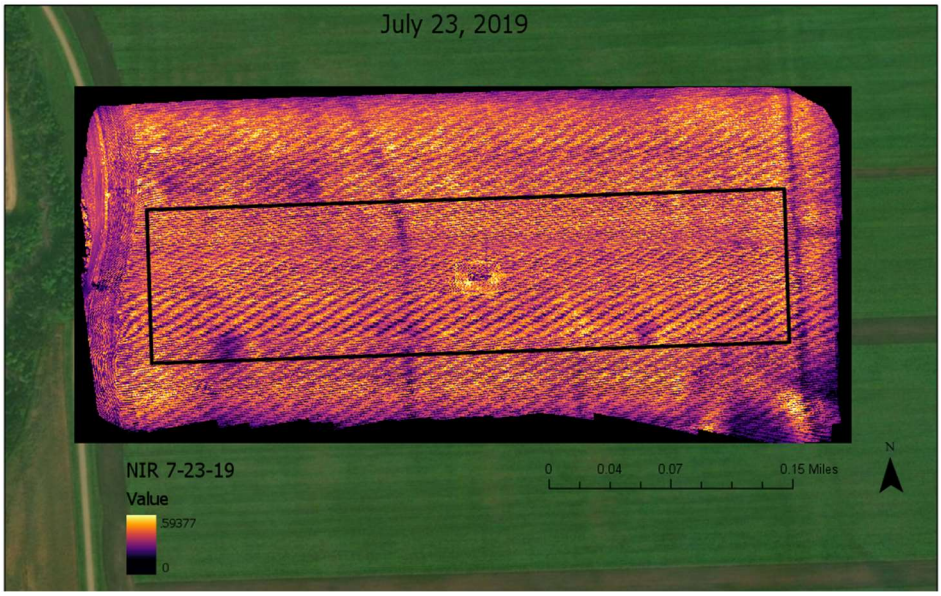

Figure 30. July 23, 2019 NIR map.

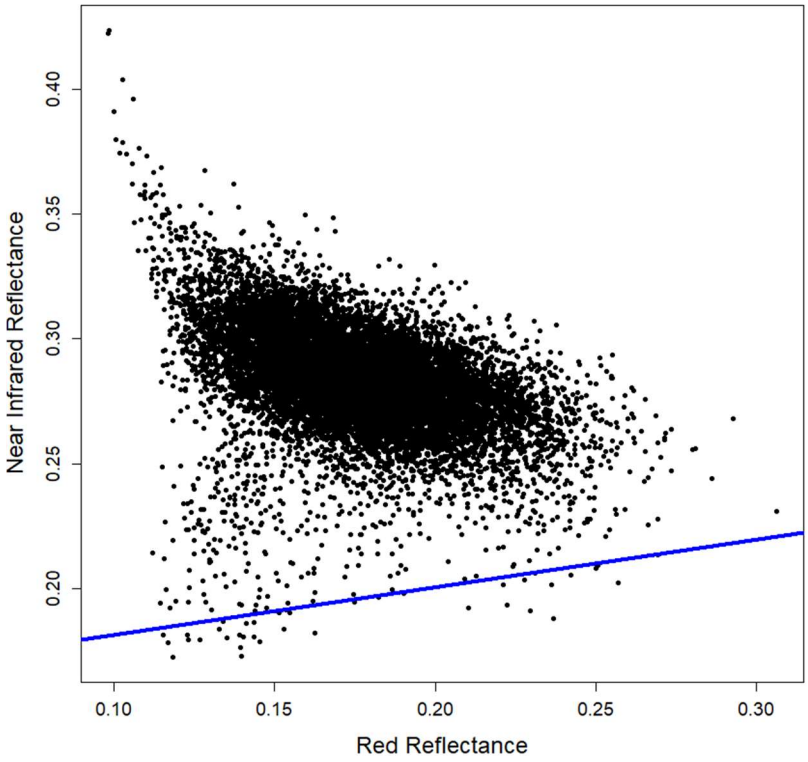

Figure 31. July 23, 2019 soil line graph.

4.2. Soil Moisture Maps

The soil moisture index maps all used the same grid to map out and average the soil moisture index in each cell point from the raster data and equation (7) along with the slope of the

soil line from each flight. The table below sums up the SM information collected from the data sets. The period after the snow melt on May 7th, showed the highest value at 0.5270 and the lowest was recorded a week after tillage on May 14th at 0.0918. Each of the four SM maps in Figures 32, 33, 34, and 35 all used the same legend for an easy comparison between data sets.

Table 2. SM map value summaries.

Date:	5/7/19	5/14/19	5/23/19	7/23/19
Average SM	0.4100	0.1551	0.3966	0.1882
SM Max	0.5270	0.2551	0.4971	0.3087
SM Min	0.2828	0.0918	0.2201	0.1122
Range	0.2442	0.1633	0.2770	0.1966
Red Average	0.2386	0.1481	0.2736	0.1758
NIR Average	0.2645	0.1609	0.2842	0.2834

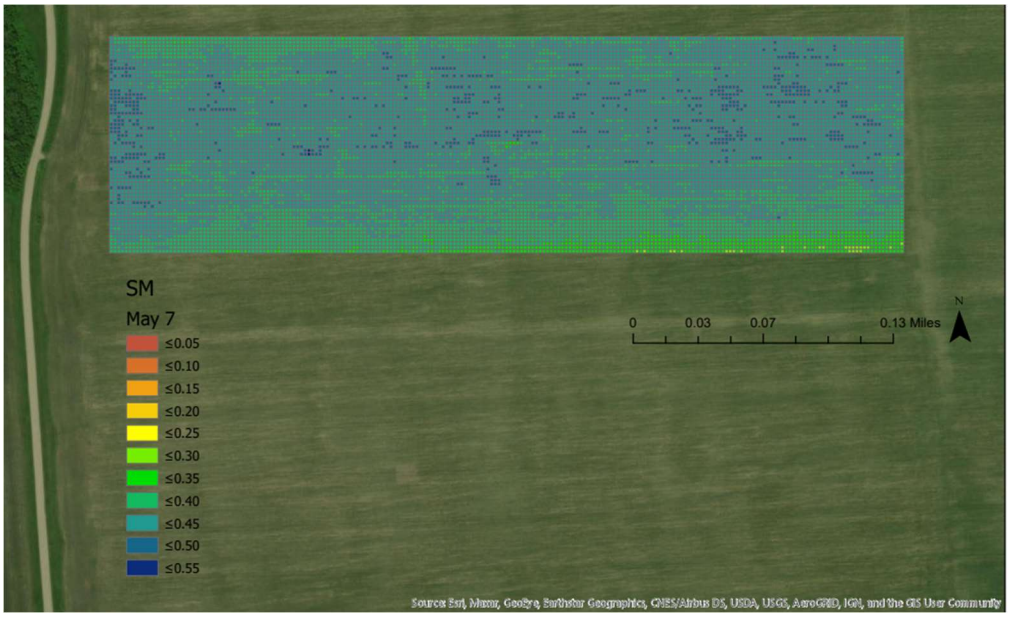

Figure 32. May 7, 2019 SM map.

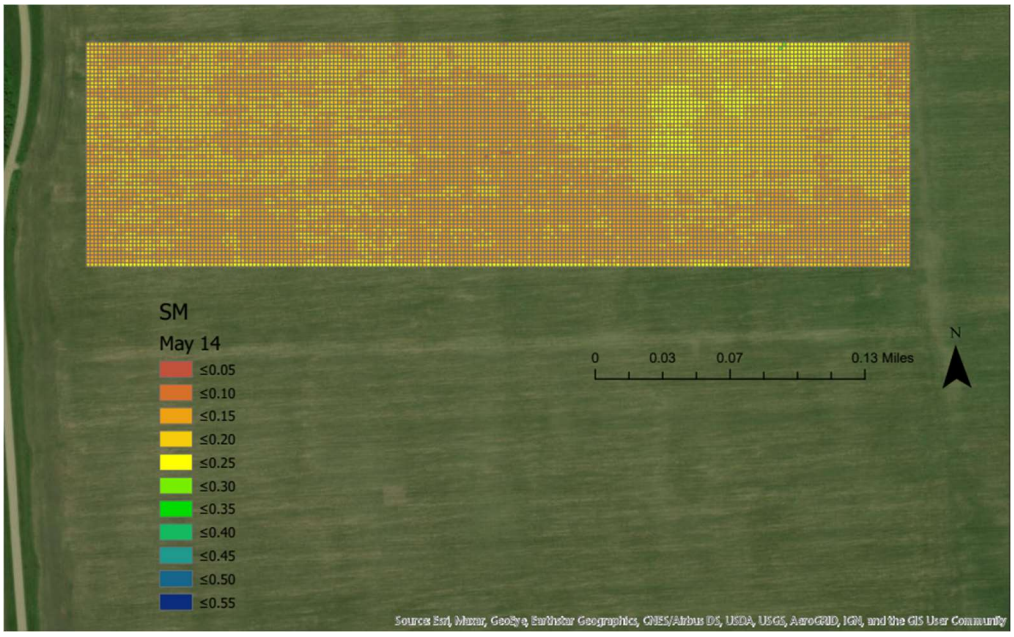

Figure 33. May 14, 2019 SM map.

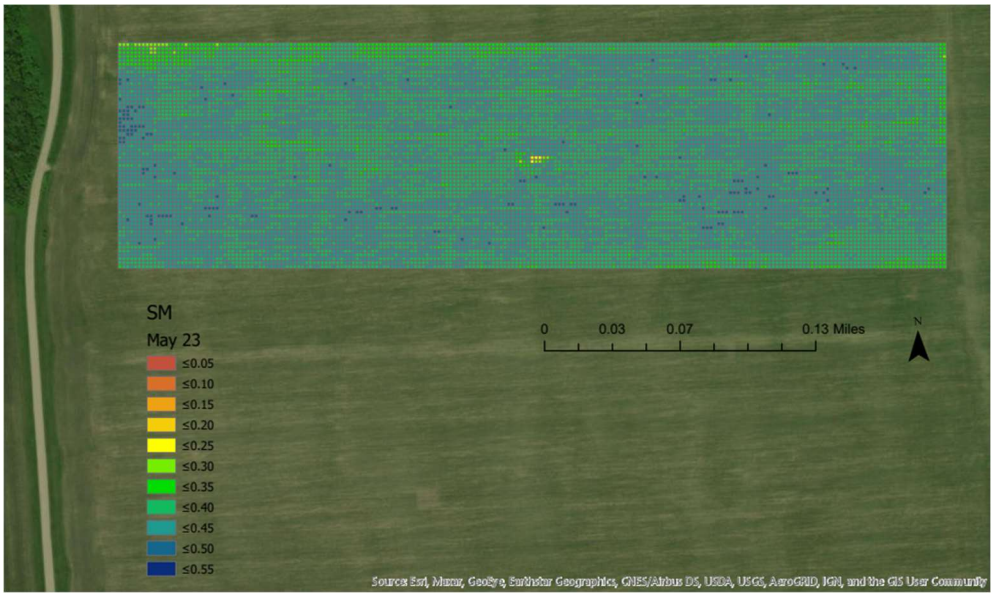

Figure 34. May 23, 2019 SM map.

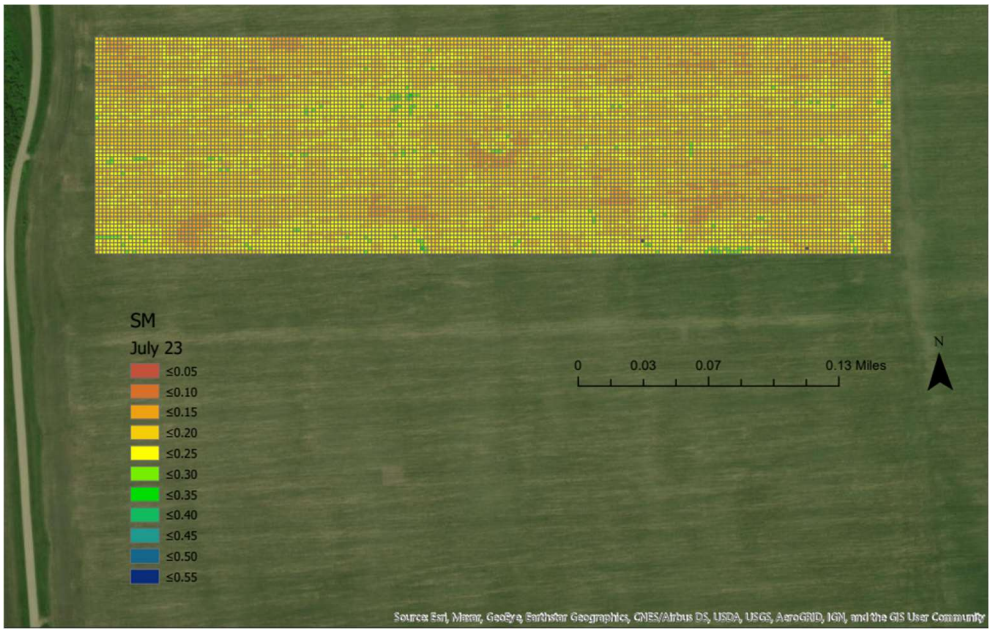

Figure 35. July 23, 2019 SM map.

4.3. TDR Data

The TDR data collected after each flight was used as a comparison data set. The 30 points of collection used the two different sizes of probes, 7.6 cm and 20 cm in length. The heavy crop residue prevented the 7.6 cm probe from gaining the best contact with the soil at some collection points. The TDR data appeared to have unachievably high values sometimes and out of range values from point to point. Below is a table of the collected data (Table 3).

Table 3. TDR collected data.

Site #	Over Tile								Between Tile							
	5/7/19		5/14/19		5/23/19		7/23/19		5/7/19		5/14/19		5/23/19		7/23/19	
	7.6 cm	20 cm	7.6 cm	20 cm	7.6 cm	20 cm	7.6 cm	20 cm	7.6 cm	20 cm	7.6 cm	20 cm	7.6 cm	20 cm	7.6 cm	20 cm
1	0.447	0.389	0.431	0.411	0.527	0.453	0.354	0.461	0.422	0.383	0.268	0.369	0.513	0.456	0.530	0.403
2	0.261	0.433	0.285	0.363	0.620	0.501	0.434	0.425	0.318	0.411	0.242	0.372	0.547	0.512	0.305	0.540
3	0.338	0.400	0.427	0.456	0.450	0.509	0.281	0.559	0.348	0.358	0.348	0.445	0.567	0.573	0.255	0.487
4	0.457	0.467	0.480	0.456	0.550	0.571	0.523	0.517	0.391	0.405	0.281	0.461	0.437	0.534	0.361	0.540
5	0.347	0.459	0.301	0.321	0.520	0.576	0.467	0.596	0.295	0.450	0.311	0.515	0.523	0.596	0.341	0.495
6	0.321	0.361	0.338	0.296	0.586	0.579	0.351	0.635	0.450	0.422	0.162	0.529	0.507	0.613	0.381	0.596
7	0.321	0.464	0.364	0.492	0.497	0.573	0.381	0.495	0.401	0.383	0.285	0.534	0.434	0.515	0.351	0.554
8	0.407	0.425	0.132	0.503	0.490	0.559	0.497	0.635	0.315	0.450	0.315	0.464	0.467	0.537	0.252	0.585
9	0.315	0.453	0.358	0.431	0.523	0.523	0.348	0.565	0.334	0.450	0.235	0.453	0.653	0.587	0.540	0.506
10	0.417	0.492	0.285	0.450	0.500	0.551	0.331	0.635	0.474	0.464	0.351	0.481	0.474	0.562	0.324	0.475
11	0.328	0.380	0.281	0.428	0.547	0.604	0.457	0.613	0.407	0.389	0.242	0.436	0.480	0.601	0.404	0.722
12	0.411	0.355	0.281	0.445	0.474	0.464	0.351	0.541	0.434	0.484	0.291	0.473	0.470	0.509	0.394	0.400
13	0.437	0.492	0.152	0.403	0.563	0.501	0.195	0.347	0.411	0.475	0.215	0.461	0.513	0.585	0.683	0.669
14	0.381	0.310	0.301	0.271	0.537	0.503	0.378	0.335	0.540	0.366	0.358	0.271	0.610	0.596	0.485	0.403
15	0.218	0.428	0.242	0.355	0.500	0.551	0.507	0.537	0.344	0.347	0.261	0.551	0.596	0.627	0.601	0.540

The larger swings and unconventional values showed a pattern of lower error in the first flight and higher error as the summer went on. This may have been a calibration issue that worsened over time.

4.4. TDR Corrected Data and Comparison

To correct the collected data by TDR, a lab experiment was conducted to correlate the values by the TDR with gravimetric soil moisture data. Soils from the same field were packed into the columns with a known bulk density of 1.25 g/cm^3, similar to the bulk density in the field. The soil was oven dried first, and a known amount of water was added to the soil to produce specified soil moisture contents. Table 4 shows the results of the lab experiment.

Table 4. TDR lab experiment results.

Experiment number		Run	Moisture content for 3 in (7.6 cm) length (%)						Moisture content for 8 in (20 cm) length (%)					
			0	15	25	35	45	53	0	15	25	35	45	53
Standard volumetric water content	1st sample	1	1.2	25.7	68.9	105.3	108.2	118.5	0.0	35.4	62.0	99.8	90.4	96.2
		2	1.2	24.2	69.4	106.2	101.7	118.5	0.0	35.1	63.4	104.5	90.4	96.2
		3	1.7	25.6	69.4	105.7	101.7	118.5	0.0	34.5	63.4	99.8	90.7	96.2
	2nd sample	4	0.0	16.9	55.2	96.4	122.4	116.5	0.0	24.8	59.0	119.0	94.8	98.7
		5	0.0	16.4	55.7	96.9	121.5	117.0	0.0	25.4	59.0	119.7	95.7	98.4
		6	0.0	16.9	55.2	96.9	122.4	116.5	0.0	24.8	59.0	120.1	95.1	98.7
	3rd sample	7	1.7	25.2	71.4	91.9	105.3	108.7	0.0	33.2	68.4	124.1	94.8	95.7
		8	1.2	26.2	71.4	92.0	106.2	111.1	0.0	33.2	68.7	124.4	95.1	95.7
		9	1.7	26.7	71.4	92.0	105.7	112.1	0.0	33.2	68.7	124.1	95.1	95.7
Average			0.97	22.64	65.33	98.14	110.57	115.27	0.00	31.07	63.51	115.06	93.57	96.83
Average Difference			-0.97	-7.64	-40.33	-63.14	-65.57	-62.27	0.00	-16.07	-38.51	-80.06	-48.57	-43.83
High clay volumetric water content	1st sample	10	2.6	19.8	48.4	72.9	73.6	78.5	2.2	22.6	50.9	83.4	78.6	83.4
		11	2.6	18.2	48.4	72.9	73.2	77.2	2.2	22.3	50.9	84.1	78.3	83.9
		12	2.6	18.6	48.4	72.9	73.2	78.9	2.2	22.3	50.9	84.1	78.9	83.4
	2nd sample	13	1.9	12.6	38.7	60.9	86.2	77.2	2.4	13.2	46.4	98.7	82.8	85.3
		14	1.6	13.5	39.1	66.6	85.2	77.5	2.4	13.0	46.4	98.7	83.9	85.6
		15	1.9	12.2	39.1	66.9	84.5	80.2	2.4	13.2	46.4	98.7	83.4	85.6
	3rd sample	16	2.3	18.9	49.4	63.0	69.9	79.9	2.3	20.4	56.2	105.3	82.8	83.9
		17	2.3	19.2	49.0	63.3	71.2	79.5	2.3	20.4	56.2	105.3	82.8	83.7
		18	2.6	19.2	49.0	63.3	73.2	79.9	2.3	20.1	56.2	105.4	82.5	83.7
Average			2.27	16.91	45.50	66.97	76.69	78.76	2.30	18.61	51.17	95.97	81.56	84.28
Average Difference			-2.27	-1.91	-20.50	-31.97	-31.69	-25.76	-2.30	-3.61	-26.17	-60.97	-36.56	-31.28

Based on the soil bulk density, the maximum water content was 53%, which was significantly lower than many of the in situ collected data points from the TDR sensor. The lab experiment showed similar discrepancies as the field measurements and remotely sensed data. Using the values from the lab experiment, a correction equation was developed from a linear fit trendline of the data. The equations formed from the lab experiment can be found in Figure 36.

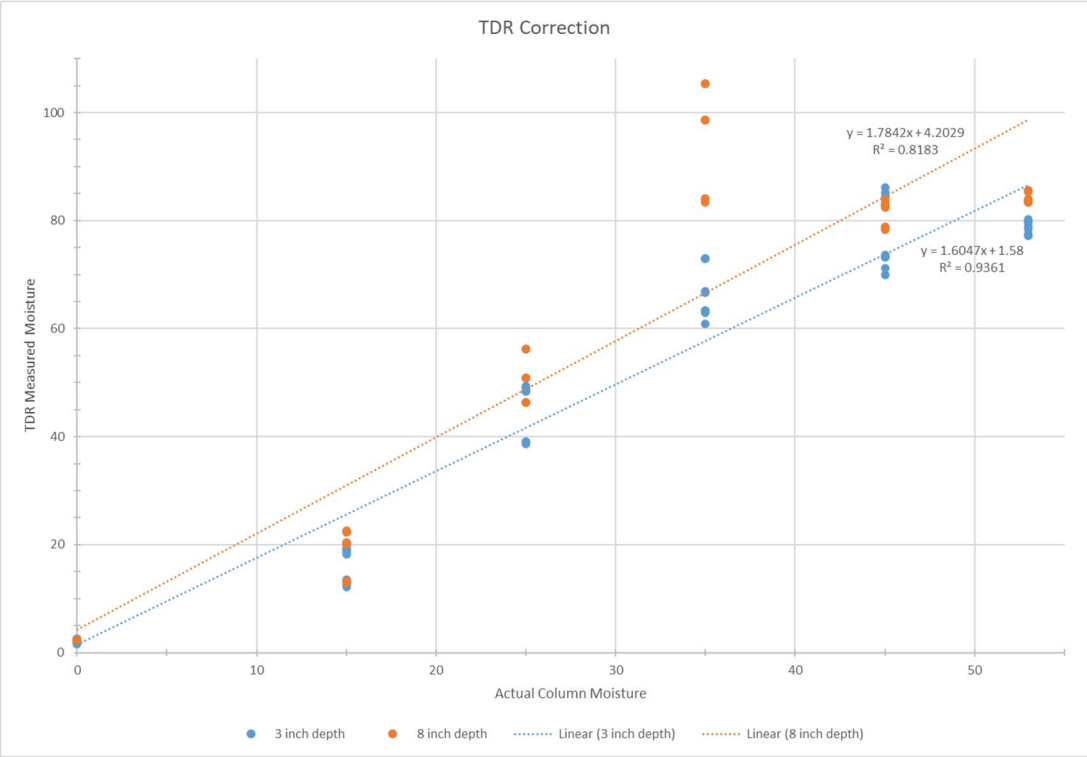

Figure 36. TDR lab experiment graph and correction equations.

Three of the four flights resulted in values that were significantly closer to the remotely sensed and the calculated values. The only flight that was worsened with the correction equation was the first flight. This anomaly raised some question as to why the first flight was close to the remotely sensed data initially and the later three flights were better with an equation to correct the data.

The first data set of comparisons are shown in Appendix A, Appendix B, and Appendix C with an average of less than a difference of 7.0 for both the 7.6 cm and 20 cm depths before

the lab correction equation was applied to the in-situ data. The average difference was increased to 20 after the correction equation was applied. The third data set can be seen in Appendix G, Appendix H, and Appendix I and showed the greatest improvement of differences averaging 38.6 in the 7.6 cm category to averaging 7.6 after lab correction. The second data set is shown in Appendix D, Appendix E, and Appendix F, and the fourth data set is shown Appendix J, Appendix K, and Appendix L and showed similar results of improvement in data after lab calibration corrections were applied to the in-situ data set.

One hypothesis is that the TDR sensor was damaged after the first data set collection which resulted in potentially skewed values for the remaining three data sets in-situ measurements. Due to the time it took to process the data, this issue was not found until much later in the project where the need for a lab analysis of the sensor and a correction equation became evident.

4.5. Results Summary

All three objectives were completed in the study with protocols developed to make soil moisture maps from UAS collected data, collecting of in-situ soil moisture data, and completing a comparison of the UAS soil moisture maps to the in-situ soil moisture measurements. From the study, four flights were successfully conducted to collect the necessary NIR and Red channel data sets. Among the flights, three were conducted over the field with limited vegetation growth, but with plenty crop residue from the previous year and one with full vegetation. Other remote sensing methods require a variability of ground conditions in the data collection area to obtain valuable results. The conditions of this field that had low variability across the data collection area led to the use of the soil moisture equation used in the study for this application. The average differences and the average percent errors of the remotely sensed data compared to the

in-situ measurements can be found in Table 5 which is a summary of Appendix A, Appendix D, Appendix G, and Appendix J. The difference and percent error 1 correlate to the values before the sensor lab calibration correction, while the difference and percent error 2 correlate to the values after the sensor lab calibration correction was applied.

The percent error was relatively consistent with the in-situ lab calibrated soil moisture data except for the data from the first flight. The first collection data set experienced the least percent error in the 20 cm depth at 9% average error and the 7.6 cm depth at 20.3% average error before sensor lab calibration, but the errors were much larger after the calibration. The range of the percent error after in-situ sensor lab calibration, excluding the first data set, was between 25.4% to 37.2%. This consistency leaned toward the need for further calibrating the remote data for better correlation. Overall, the limited four data sets showed plausible and promising results but need more investigating to understand the percent error trend in better detail.

Looking at the different data sets, it was quite evident when a weather event or farming event took place. The snow melts and heavy rainfall caused soil moisture to increase, which were noticeable in the imagery on both the first data set and the third data set. The second data set, the driest data set, coincided well with the field work during tillage and planting practices that took place right before the data collection. Even with the last data set experiencing a completely different condition of vegetation, more data sets in different conditions would be beneficial.

Table 5. Comparison summaries.

Date	Remote Sensed	In Situ Avg		Difference 1 Avg		Percent Error 1 Avg		Corrected In Situ Avg		Difference 2 Avg		Percent Error 2 Avg	
		7.6 cm	20 cm	7.6 cm Δ	20 cm Δ	7.6 cm	20 cm	7.6 cm	20 cm	7.6 cm Δ	20 cm Δ	7.6 cm	20 cm
5/7/2019	41.7	37.6	41.8	6.7	3.7	20.3%	9.0%	22.5	21.1	19.3	20.7	93.0%	100.5%
5/14/2019	13.9	29.4	43.0	15.5	29.1	48.7%	66.6%	17.3	21.7	4.8	8.0	27.6%	34.4%
5/23/2019	38.6	52.3	54.7	13.6	16.1	25.3%	29.1%	31.6	28.3	7.6	10.3	25.4%	37.2%
7/23/2019	17.9	40.2	52.7	22.3	34.8	52.5%	64.7%	24.1	27.2	7.2	8.1	28.1%	33.8%

Averages summarized from Appendix A, Appendix D, Appendix G, and Appendix J

5. CONCLUSION

A field study was conducted in 2019 at a tile drained farm field in Clay County, MN. Four UAS flights were carried over by a DJI Matric 600 from the spring with no vegetation to the middle of the growing season with full vegetable. Multispectral images by a Micasense Altum sensor and its gimbal and thermal images by a FLIR Zenmuse XTS sensor were collected and processed. The soil moisture maps were developed using data from Red and NIR imagery with assistance from Pix4D, ArcGIS, and R Statistics software. During each UAS flight, in-situ soil moisture data were measured at 7.6 cm and 20 cm depths from 30 fixed locations in the field. A simple comparison between the UAS soil moisture and in-situ soil moisture showed a good agreement for the first flight, but not for the rest. Another lab experiment was conducted to calibrate the soil moisture sensor against the gravitational method. The results showed that after the calibration of the sensor, the soil moisture data from the UAS method were comparable with the in-situ soil moisture data. This indicated that the UAS collected images were capable of developing soil moisture maps in a timely manner. A simple protocol on how to create the soil moisture map was developed so that others may follow. However, it became challenging and time consuming for an average producer to use this technology to map their fields quickly following the protocol. The major limiting factors are the large amount of computing power needed to process the large data sets, the need to use remote servers for data processing, and specifically, various programs required to determine the input parameters.

Further studies in different conditions, including drier and wetter parameters and different crop conditions, are needed to refine the data and the method. This would further the understanding of limitations to the soil moisture equation. A computer program may be

developed to simplify the map development process so that an end user can easily apply the technology and develop a soil moisture map in a timely manner.

REFERENCES

Amani, M., Parsian, S., MirMazloumi, S. M., & Aineh, O. (2015). Two new soil moisture indices based on NIR-red triangle space of Landsat-8 data. *International Journal of Applied Earth Observation and Geoinformation*, 176-186.

Amani, M., Salehi, B., Mahdavi, S., Masjedi, A., & Dehnavi, S. (2017). Temperature-Vegetation-soil Moisture Dryness Index (TVMDI). *Remote Sensing of Enviroment*, 197 1-14.

Chang, K.-T., & Hsu, W.-L. (2018). Estimating Soil Moisture Content Using Unmanned Aerial Vehicles Equipped with Thermal Infrared Sensors. *Proceedings of IEEE International Conference on Applied System Innovation 2018* (pp. 168-171). Chiba: Institute of Electrical and Electronics Engineers, Inc.

Engman, E. T. (2000). Soil Moisture. In G. A. Schultz, & E. T. Engman, *Remote Sensing in Hydrology and Water Managment* (pp. 197-216). Berlin: Springer.

Entekhabi, D., Njoku, E. G., O'Neill, P. E., Kellogg, K. H., Crow, W. T., Edelstein, W. N., . . . Zyl, J. V. (2010). The Soil Moisture Active Passive (SMAP) Mission. *Proceedings of the IEEE*, 704-716.

Evans, R., Cassel, D., & Sneed, R. E. (1996, June). *Measuring Soil Water for Irrigation Scheduling: Monitoring Methods and Devices.* Retrieved from NC State Extention: https://content.ces.ncsu.edu/measuring-soil-water-for-irrigation-scheduling

Hassen-Esfahani, L., Ebtehaj, A. M., Torres-Rua, A., & McKee, M. (2017). Spatial Scale Gap Filling Using an Unmanned Aerial System: A Statistical Downscaling Method for Applications in Precision Agriculture. *Sensors*, doi:10.3390/s17092106.

Hillel, D. (1998). *Enviromental Soil Physics.* San Diego: Academic Press.

Kolars, K., Jia, X., Steele, D.D., and Scherer, T.F. (2019). A soil water balance model for subsurface water management. *Applied Engineering in Agriculture* 35(4): 633-646.

Kuenzer, C., & Dech, S. (2013). *Thermal Infrared Remote Sensing.* Dordrecht: Springer.

Kuenzer, C., Gessner, U., & Wagner, W. (2013). Soil Moisture from Thermal Infrared Satellite Data: Synergies with Microwave Data. In C. Kuenzer, & S. Dech, *Thermal Infrared Remote Sensing: Sensors, Methods, Applications* (pp. 315-330). Dordrecht: Springer.

Lakshmi, V. (2017). *Remote Sensing of Hydrological Extremes.* Springer International Publishing.

Lambin, E. F., & Ehrlich, D. (1996). The surface temperature-vegetation index space for land cover and land cover change analysis. *International Journal of Remote Sensing*, 463-487.

Leng, P., Li, Z.-L., Duan, S.-B., Gao, M.-F., & Huo, H.-Y. (2018). First results of all-weather soil moisture retrieval from an optical/thermal infrared remote-sensing based operational system in China. *Internation Journal of Remote Sensing*, DOI:10.1080/01431161.2018.1468119.

Ma, H., Zeng, J., Chen, N., Zhang, X., Cosh, M. H., & Wang, W. (2019). Satellite surface soil moisture from SMAP, SMOS, AMSR2 and ESA CCI: A comprehensive assessment using global ground-based obseravtions. *Remote Sensing of Enviroment, 231*. doi:https://doi.org/10.1016/j.rse.2019.111215

"topography." *Merriam-Webster.com*. 2019 Retrieved Dec 1, 2019, from https://www.merriam-webster.com/dictionary/topography

Niaghi, A. R., **Jia**, X., Steele, D.D., and Scherer, T.F. (2019). Drainage water management effects on energy flux partitioning, evapotranspiration, and crop coefficients for corn. *Agricultural Water Management* 225 (2019) 105760. https://doi.org/10.1016/j.agwat.2019.105760.

Pietroniro, A., Toyra, J., Leconte, R., & Kite, G. (2005). Remote Sensing of Surface Water and Soil Moisture. In C. R. Duguay, & A. Pietroniro, *Remote Sensing in Northern Hydrology* (pp. 119-142). Washington D.C.: American Geophysical Union.

Quebajo, L., Perez-Ruiz, M., Perez-Urrestarazu, L., Marinez, G., & Egea, G. (2018). Linking thermal imaging and soil remote sensing to enhance irrigation management of sugar beet. *Biosystems Engineering*, 77-87.

Rijal, S., Zhang, X., & Jia, X. (2012). Estimating Surface Soil Water Content in the Red River Valley of the North using Landsat 5 TM Data. *Soil Science Journal of America*.

Sandholt, I., Rasmussen, K., & Andersen, J. (2001). A simple interpretation of the surface temperature/vegetation index space for assessment of surface moisture status. *Remote Sensing of Enviroment*, 213-224.

Santhosh, S. K., Laguette, S., Casady, G. M., & Seielstad, G. A. (2003). Remote sensing applications for precision agriculture: A learning community approach. *Remonte Sensing of Enviroment*, 157-169.

Sudha Lekshmi, S., Singh, D., & Baghini, M. S. (2014). A critical review of soil moisture measurement. *Measurement*, 92-105.

USDA. (2018, November). *Web Soil Survey*. Retrieved from https://websoilsurvey.sc.egov.usda.gov/App/WebSoilSurvey.aspx

Wigmore, O., Mark, B., McKenzie, J., Baraer, M., & Lautz, L. (2019). Sub-metre mapping of surface soil moisture in proglacial valleys of the tropical Andes using a multispecral unmanned aerial vehicle. *Remote Sensing of Enviroment, 222*, 104-118.

APPENDIX A. MAY 7, 2019 RESULTS

	5/7/19	In Situ		Difference 1		Percent Error 1		Corrected In Situ		Difference 2		Percent Error 2	
Site	Remote	7.6 cm	20 cm	7.6 cm Δ	20 cm Δ	7.6 cm	20 cm	7.6 cm	20 cm	7.6 cm Δ	20 cm Δ	7.6 cm	20 cm
1	34	44.7	38.9	10.7	4.9	23.9%	12.6%	26.87	19.45	7.13	14.55	26.5%	74.8%
2	41	26.1	43.3	14.9	2.3	57.1%	5.3%	15.28	21.91	25.72	19.09	168.3%	87.1%
3	42	33.8	40	8.2	2	24.3%	5.0%	20.08	20.06	21.92	21.94	109.2%	109.3%
4	48	45.7	46.7	2.3	1.3	5.0%	2.8%	27.49	23.82	20.51	24.18	74.6%	101.5%
5	43	34.7	45.9	8.3	2.9	23.9%	6.3%	20.64	23.37	22.36	19.63	108.3%	84.0%
6	43	32.1	36.1	10.9	6.9	34.0%	19.1%	19.02	17.88	23.98	25.12	126.1%	140.5%
7	42	32.1	46.4	9.9	4.4	30.8%	9.5%	19.02	23.65	22.98	18.35	120.8%	77.6%
8	45	40.7	42.5	4.3	2.5	10.6%	5.9%	24.38	21.46	20.62	23.54	84.6%	109.6%
9	41	31.5	45.3	9.5	4.3	30.2%	9.5%	18.65	23.03	22.35	17.97	119.9%	78.0%
10	45	41.7	49.2	3.3	4.2	7.9%	8.5%	25.00	25.22	20.00	19.78	80.0%	78.4%
11	42	32.8	38	9.2	4	28.0%	10.5%	19.46	18.94	22.54	23.06	115.9%	121.7%
12	41	41.1	35.5	0.1	5.5	0.2%	15.5%	24.63	17.54	16.37	23.46	66.5%	133.7%
13	44	43.7	49.2	0.3	5.2	0.7%	10.6%	26.25	25.22	17.75	18.78	67.6%	74.5%
14	37	38.1	31	1.1	6	2.9%	19.4%	22.76	15.02	14.24	21.98	62.6%	146.3%
15	39	21.8	42.8	17.2	3.8	78.9%	8.9%	12.60	21.63	26.40	17.37	209.5%	80.3%
16	44	42.2	38.3	1.8	5.7	4.3%	14.9%	25.31	19.11	18.69	24.89	73.8%	130.2%
17	40	31.8	41.1	8.2	1.1	25.8%	2.7%	18.83	20.68	21.17	19.32	112.4%	93.4%
18	44	34.8	35.8	9.2	8.2	26.4%	22.9%	20.70	17.71	23.30	26.29	112.5%	148.5%
19	42	39.1	40.5	2.9	1.5	7.4%	3.7%	23.38	20.34	18.62	21.66	79.6%	106.5%
20	44	29.5	45	14.5	1	49.2%	2.2%	17.40	22.87	26.60	21.13	152.9%	92.4%
21	44	45	42.2	1	1.8	2.2%	4.3%	27.06	21.30	16.94	22.70	62.6%	106.6%
22	43	40.1	38.3	2.9	4.7	7.2%	12.3%	24.00	19.11	19.00	23.89	79.1%	125.0%
23	45	31.5	45	13.5	0	42.9%	0.0%	18.65	22.87	26.35	22.13	141.3%	96.8%
24	41	33.4	45	7.6	4	22.8%	8.9%	19.83	22.87	21.17	18.13	106.8%	79.3%
25	44	47.4	46.4	3.4	2.4	7.2%	5.2%	28.55	23.65	15.45	20.35	54.1%	86.0%
26	38	40.7	38.9	2.7	0.9	6.6%	2.3%	24.38	19.45	13.62	18.55	55.9%	95.4%
27	40	43.4	48.4	3.4	8.4	7.8%	17.4%	26.06	24.77	13.94	15.23	53.5%	61.5%
28	41	41.1	47.5	0.1	6.5	0.2%	13.7%	24.63	24.27	16.37	16.73	66.5%	69.0%
29	37	54	36.6	17	0.4	31.5%	1.1%	32.67	18.16	4.33	18.84	13.3%	103.8%
30	38	34.4	34.7	3.6	3.3	10.5%	9.5%	20.45	17.09	17.55	20.91	85.8%	122.3%
Average:	41.7	37.6	41.8	6.7	3.7	20.3%	9.0%	22.5	21.1	19.3	20.7	93.0%	100.5%

APPENDIX B. 7.6 CM DEPTH COMPARISON

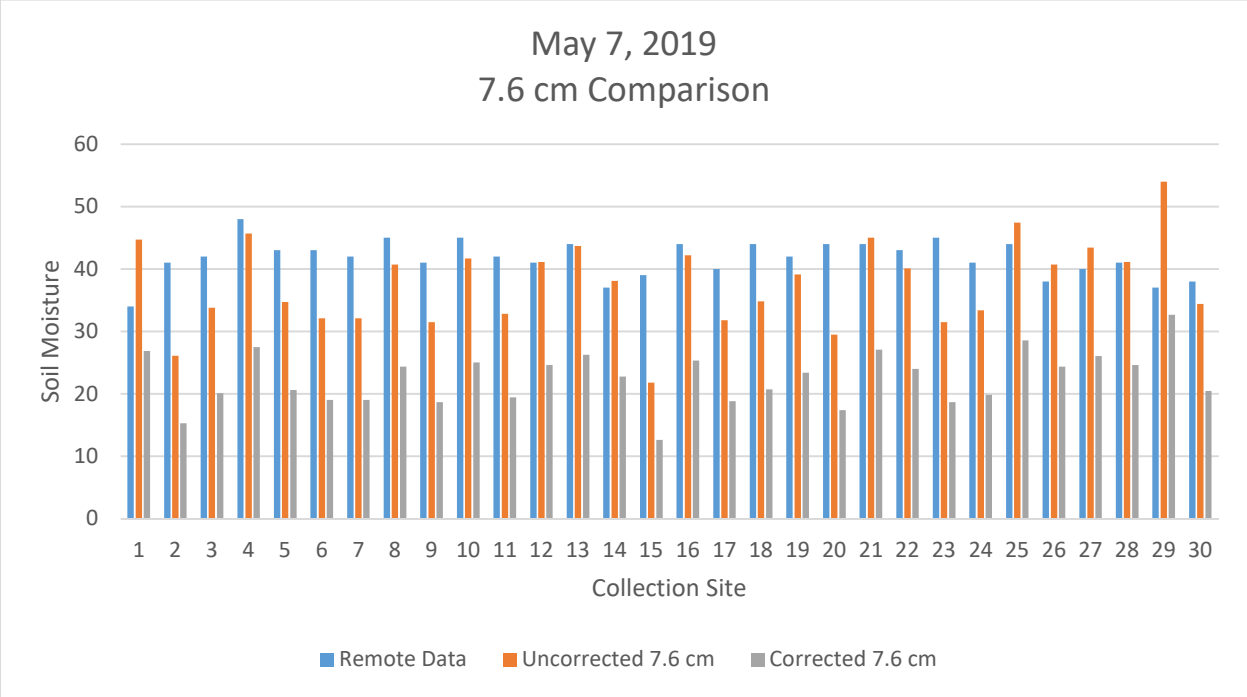

APPENDIX C. 20 CM DEPTH COMPARISON

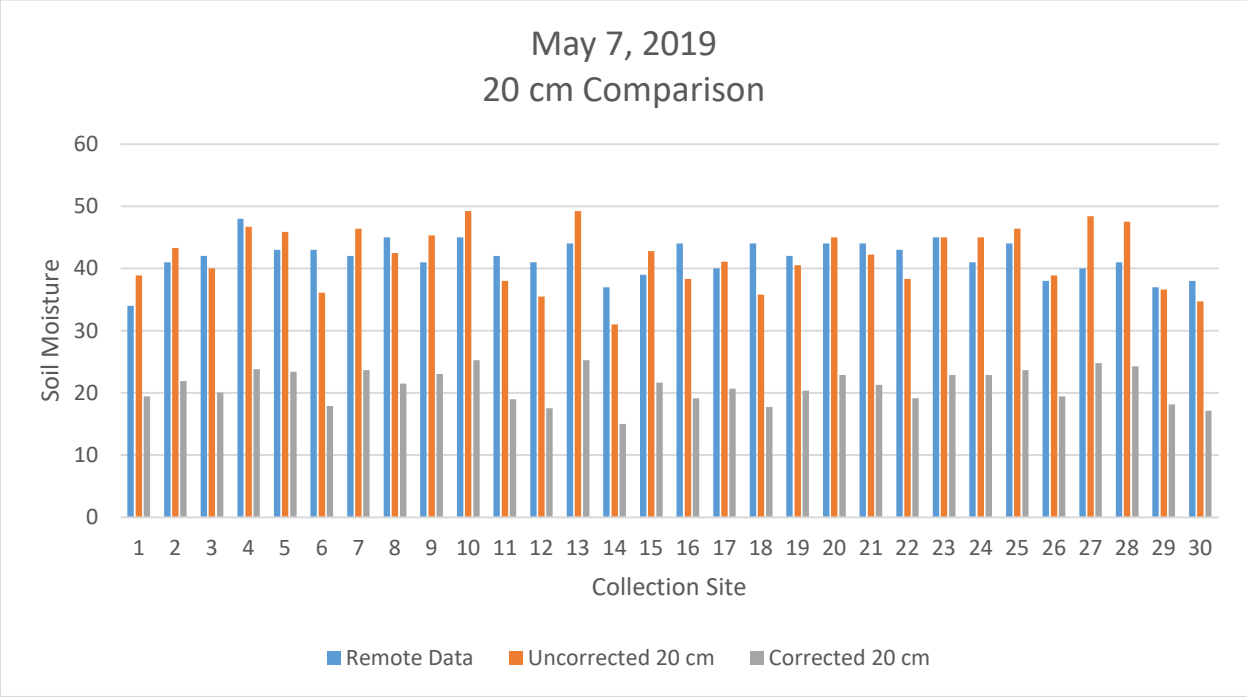

APPENDIX D. MAY 14, 2019 RESULTS

	5/14/19	In Situ		Difference 1		Percent Error 1		Corrected In Situ		Difference 2		Percent Error 2	
Site	Remote	7.6 cm	20 cm	7.6 cm Δ	20 cm Δ	7.6 cm	20 cm	7.6 cm	20 cm	7.6 cm Δ	20 cm Δ	7.6 cm	20 cm
1	10	43.1	41.1	33.1	31.1	76.8%	75.7%	25.87	20.68	15.87	10.68	61.4%	51.6%
2	15	28.5	36.3	13.5	21.3	47.4%	58.7%	16.78	17.99	1.78	2.99	10.6%	16.6%
3	13	42.7	45.6	29.7	32.6	69.6%	71.5%	25.62	23.20	12.62	10.20	49.3%	44.0%
4	15	48	45.6	33	30.6	68.8%	67.1%	28.93	23.20	13.93	8.20	48.1%	35.4%
5	14	30.1	32.1	16.1	18.1	53.5%	56.4%	17.77	15.64	3.77	1.64	21.2%	10.5%
6	15	33.8	29.6	18.8	14.6	55.6%	49.3%	20.08	14.23	5.08	0.77	25.3%	5.4%
7	13	36.4	49.2	23.4	36.2	64.3%	73.6%	21.70	25.22	8.70	12.22	40.1%	48.5%
8	13	13.2	50.3	0.2	37.3	1.5%	74.2%	7.24	25.84	5.76	12.84	79.5%	49.7%
9	14	35.8	43.1	21.8	29.1	60.9%	67.5%	21.32	21.80	7.32	7.80	34.3%	35.8%
10	15	28.5	45	13.5	30	47.4%	66.7%	16.78	22.87	1.78	7.87	10.6%	34.4%
11	15	28.1	42.8	13.1	27.8	46.6%	65.0%	16.53	21.63	1.53	6.63	9.2%	30.7%
12	14	28.1	44.5	14.1	30.5	50.2%	68.5%	16.53	22.59	2.53	8.59	15.3%	38.0%
13	15	15.2	40.3	0.2	25.3	1.3%	62.8%	8.49	20.23	6.51	5.23	76.7%	25.9%
14	14	30.1	27.1	16.1	13.1	53.5%	48.3%	17.77	12.83	3.77	1.17	21.2%	9.1%
15	14	24.2	35.5	10.2	21.5	42.1%	60.6%	14.10	17.54	0.10	3.54	0.7%	20.2%
16	14	26.8	36.9	12.8	22.9	47.8%	62.1%	15.72	18.33	1.72	4.33	10.9%	23.6%
17	13	24.2	37.2	11.2	24.2	46.3%	65.1%	14.10	18.49	1.10	5.49	7.8%	29.7%
18	14	34.8	44.5	20.8	30.5	59.8%	68.5%	20.70	22.59	6.70	8.59	32.4%	38.0%
19	13	28.1	46.1	15.1	33.1	53.7%	71.8%	16.53	23.48	3.53	10.48	21.3%	44.6%
20	14	31.1	51.5	17.1	37.5	55.0%	72.8%	18.40	26.51	4.40	12.51	23.9%	47.2%
21	15	16.2	52.9	1.2	37.9	7.4%	71.6%	9.11	27.29	5.89	12.29	64.6%	45.0%
22	13	28.5	53.4	15.5	40.4	54.4%	75.7%	16.78	27.57	3.78	14.57	22.5%	52.9%
23	14	31.5	46.4	17.5	32.4	55.6%	69.8%	18.65	23.65	4.65	9.65	24.9%	40.8%
24	14	23.5	45.3	9.5	31.3	40.4%	69.1%	13.66	23.03	0.34	9.03	2.5%	39.2%
25	15	35.1	48.1	20.1	33.1	57.3%	68.8%	20.89	24.60	5.89	9.60	28.2%	39.0%
26	13	24.2	43.6	11.2	30.6	46.3%	70.2%	14.10	22.08	1.10	9.08	7.8%	41.1%
27	14	29.1	47.3	15.1	33.3	51.9%	70.4%	17.15	24.16	3.15	10.16	18.4%	42.0%
28	14	21.5	46.1	7.5	32.1	34.9%	69.6%	12.41	23.48	1.59	9.48	12.8%	40.4%
29	13	35.8	27.1	22.8	14.1	63.7%	52.0%	21.32	12.83	8.32	0.17	39.0%	1.3%
30	14	26.1	55.1	12.1	41.1	46.4%	74.6%	15.28	28.53	1.28	14.53	8.4%	50.9%
Average:	13.9	29.4	43.0	15.5	29.1	48.7%	66.6%	17.3	21.7	4.8	8.0	27.6%	34.4%

APPENDIX E. 7.6 CM DEPTH COMPARISON

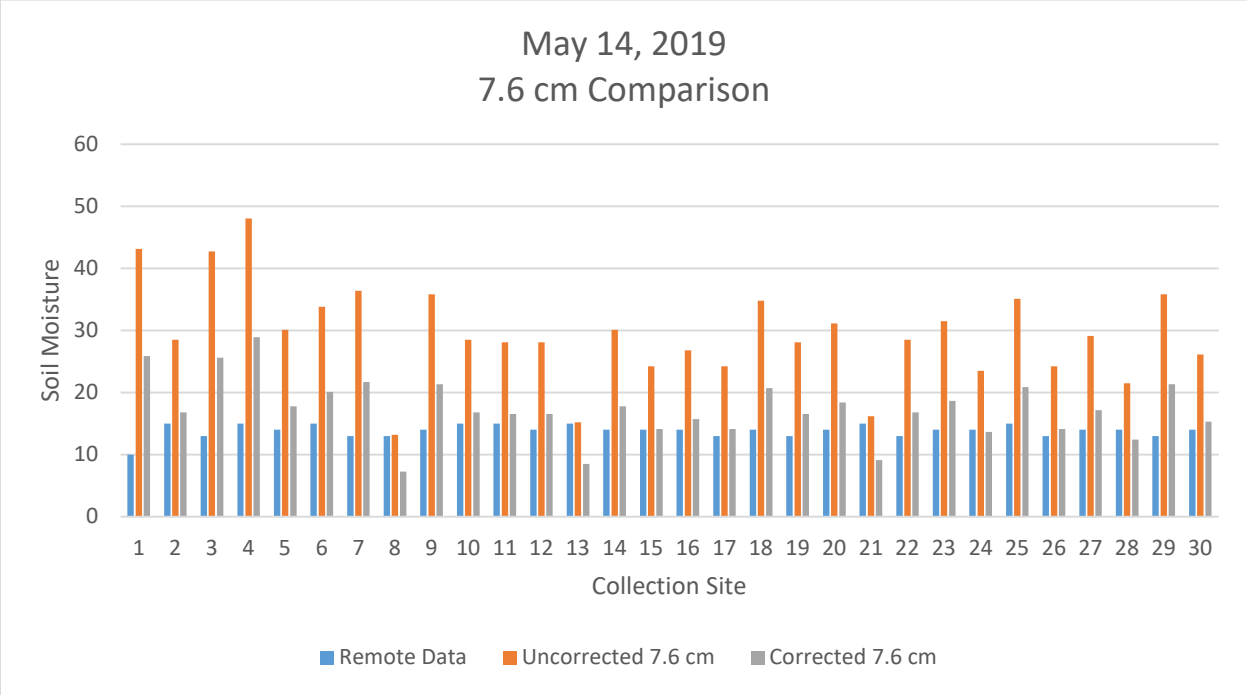

APPENDIX F. 20 CM DEPTH COMPARISON

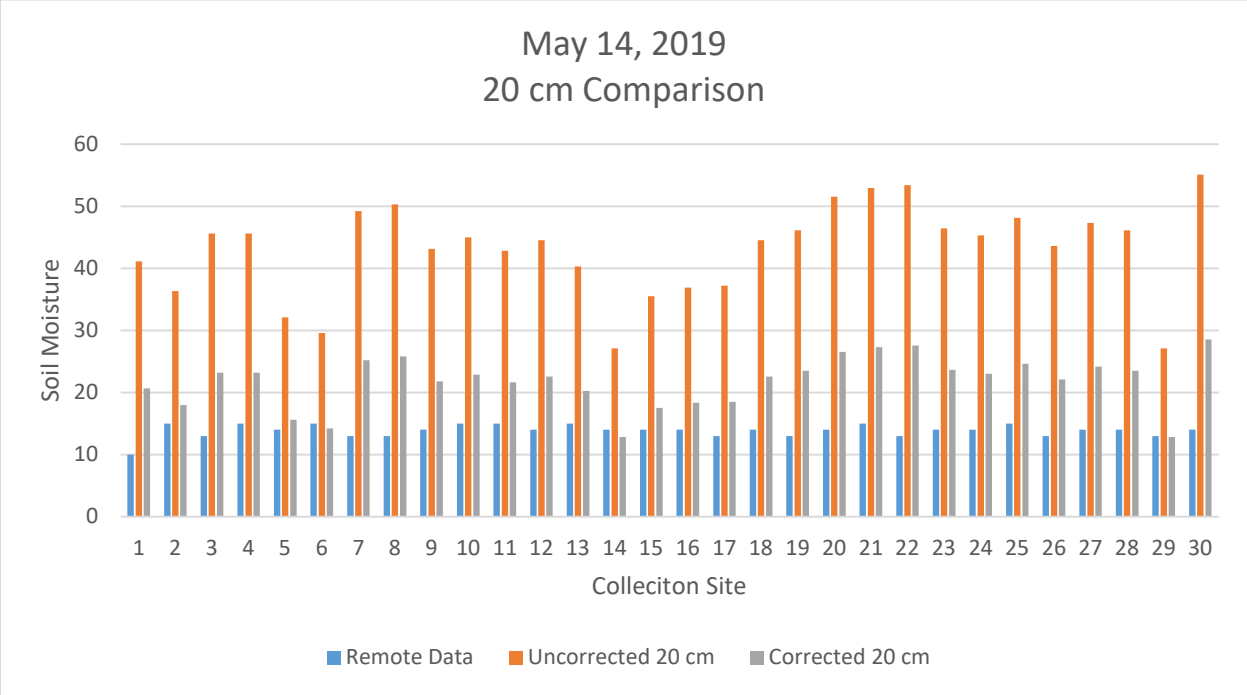

APPENDIX G. MAY 23, 2019 RESULTS

	5/23/19	In Situ		Difference 1		Percent Error 1		Corrected In Situ		Difference 2		Percent Error 2	
Site	Remote	7.6 cm	20 cm	7.6 cm Δ	20 cm Δ	7.6 cm	20 cm	7.6 cm	20 cm	7.6 cm Δ	20 cm Δ	7.6 cm	20 cm
1	40	52.7	45.3	12.7	5.3	24.1%	11.7%	31.86	23.03	8.14	16.97	25.6%	73.7%
2	40	62	50.1	22	10.1	35.5%	20.2%	37.65	25.72	2.35	14.28	6.2%	55.5%
3	37	45	50.9	8	13.9	17.8%	27.3%	27.06	26.17	9.94	10.83	36.7%	41.4%
4	42	55	57.1	13	15.1	23.6%	26.4%	33.29	29.65	8.71	12.35	26.2%	41.7%
5	41	52	57.6	11	16.6	21.2%	28.8%	31.42	29.93	9.58	11.07	30.5%	37.0%
6	42	58.6	57.9	16.6	15.9	28.3%	27.5%	35.53	30.10	6.47	11.90	18.2%	39.6%
7	40	49.7	57.3	9.7	17.3	19.5%	30.2%	29.99	29.76	10.01	10.24	33.4%	34.4%
8	42	49	55.9	7	13.9	14.3%	24.9%	29.55	28.98	12.45	13.02	42.1%	45.0%
9	42	52.3	52.3	10.3	10.3	19.7%	19.7%	31.61	26.96	10.39	15.04	32.9%	55.8%
10	43	50	55.1	7	12.1	14.0%	22.0%	30.17	28.53	12.83	14.47	42.5%	50.7%
11	38	54.7	60.4	16.7	22.4	30.5%	37.1%	33.10	31.50	4.90	6.50	14.8%	20.6%
12	37	47.4	46.4	10.4	9.4	21.9%	20.3%	28.55	23.65	8.45	13.35	29.6%	56.4%
13	40	56.3	50.1	16.3	10.1	29.0%	20.2%	34.10	25.72	5.90	14.28	17.3%	55.5%
14	35	53.7	50.3	18.7	15.3	34.8%	30.4%	32.48	25.84	2.52	9.16	7.8%	35.5%
15	38	50	55.1	12	17.1	24.0%	31.0%	30.17	28.53	7.83	9.47	25.9%	33.2%
16	25	51.3	45.6	26.3	20.6	51.3%	45.2%	30.98	23.20	5.98	1.80	19.3%	7.7%
17	38	54.7	51.2	16.7	13.2	30.5%	25.8%	33.10	26.34	4.90	11.66	14.8%	44.3%
18	36	56.7	57.3	20.7	21.3	36.5%	37.2%	34.35	29.76	1.65	6.24	4.8%	21.0%
19	40	43.7	53.4	3.7	13.4	8.5%	25.1%	26.25	27.57	13.75	12.43	52.4%	45.1%
20	40	52.3	59.6	12.3	19.6	23.5%	32.9%	31.61	31.05	8.39	8.95	26.6%	28.8%
21	38	50.7	61.3	12.7	23.3	25.0%	38.0%	30.61	32.00	7.39	6.00	24.1%	18.7%
22	38	43.4	51.5	5.4	13.5	12.4%	26.2%	26.06	26.51	11.94	11.49	45.8%	43.3%
23	39	46.7	53.7	7.7	14.7	16.5%	27.4%	28.12	27.74	10.88	11.26	38.7%	40.6%
24	37	65.3	58.7	28.3	21.7	43.3%	37.0%	39.71	30.54	2.71	6.46	6.8%	21.1%
25	41	47.4	56.2	6.4	15.2	13.5%	27.0%	28.55	29.14	12.45	11.86	43.6%	40.7%
26	38	48	60.1	10	22.1	20.8%	36.8%	28.93	31.33	9.07	6.67	31.4%	21.3%
27	36	47	50.9	11	14.9	23.4%	29.3%	28.30	26.17	7.70	9.83	27.2%	37.5%
28	41	51.3	58.5	10.3	17.5	20.1%	29.9%	30.98	30.43	10.02	10.57	32.3%	34.7%
29	39	61	59.6	22	20.6	36.1%	34.6%	37.03	31.05	1.97	7.95	5.3%	25.6%
30	36	59.6	62.7	23.6	26.7	39.6%	42.6%	36.16	32.79	0.16	3.21	0.4%	9.8%
Average:	38.6	52.3	54.7	13.6	16.1	25.3%	29.1%	31.6	28.3	7.6	10.3	25.4%	37.2%

APPENDIX H. 7.6 CM DEPTH COMPARISON

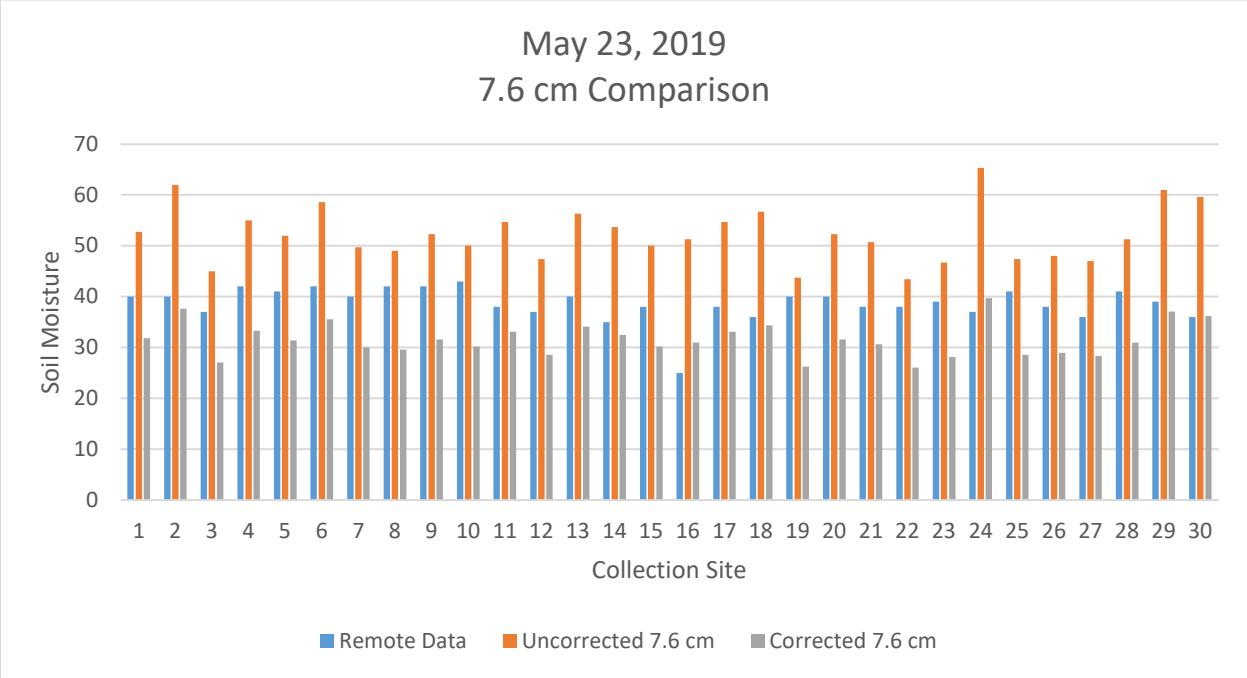

APPENDIX I. 20 CM DEPTH COMPARISON

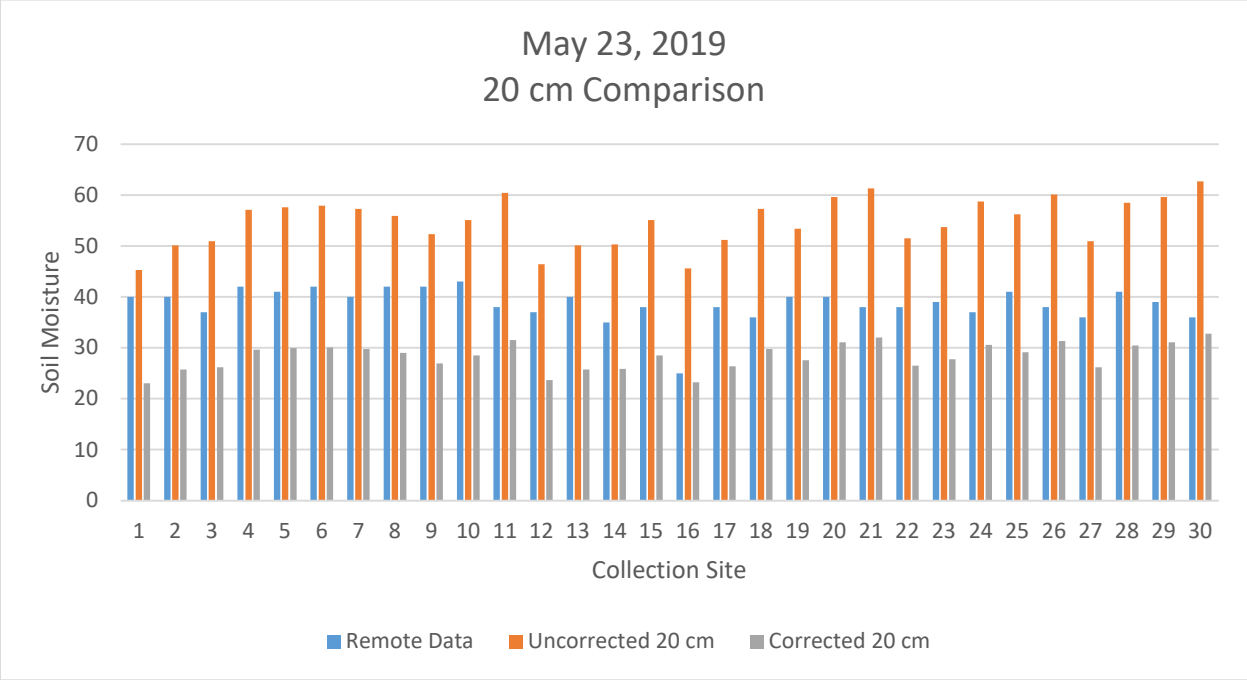

APPENDIX J. JULY 23, 2019 RESULTS

	7/23/19	In Situ		Difference 1		Percent Error 1		Corrected In Situ		Difference 2		Percent Error 2	
Site	Remote	7.6 cm	20 cm	7.6 cm Δ	20 cm Δ	7.6 cm	20 cm	7.6 cm	20 cm	7.6 cm Δ	20 cm Δ	7.6 cm	20 cm
1	20	35.4	46.1	15.4	26.1	43.5%	56.6%	21.08	23.48	1.08	2.62	5.1%	14.8%
2	19	43.4	42.5	24.4	23.5	56.2%	55.3%	26.06	21.46	7.06	2.04	27.1%	11.5%
3	19	28.1	55.9	9.1	36.9	32.4%	66.0%	16.53	28.98	2.47	7.92	15.0%	34.4%
4	19	52.3	51.7	33.3	32.7	63.7%	63.2%	31.61	26.62	12.61	6.08	39.9%	28.6%
5	14	46.7	59.6	32.7	45.6	70.0%	76.5%	28.12	31.05	14.12	14.55	50.2%	54.9%
6	20	35.1	63.5	15.1	43.5	43.0%	68.5%	20.89	33.23	0.89	10.27	4.3%	39.8%
7	19	38.1	49.5	19.1	30.5	50.1%	61.6%	22.76	25.39	3.76	5.11	16.5%	25.2%
8	22	49.7	63.5	27.7	41.5	55.7%	65.4%	29.99	33.23	7.99	8.27	26.6%	33.8%
9	17	34.8	56.5	17.8	39.5	51.1%	69.9%	20.70	29.31	3.70	10.19	17.9%	42.0%
10	13	33.1	63.5	20.1	50.5	60.7%	79.5%	19.64	33.23	6.64	17.27	33.8%	60.9%
11	16	45.7	61.3	29.7	45.3	65.0%	73.9%	27.49	32.00	11.49	13.30	41.8%	50.0%
12	17	35.1	54.1	18.1	37.1	51.6%	68.6%	20.89	27.97	3.89	9.13	18.6%	39.2%
13	18	19.5	34.7	1.5	16.7	7.7%	48.1%	11.17	17.09	6.83	0.39	61.2%	5.3%
14	17	37.8	33.5	20.8	16.5	55.0%	49.3%	22.57	16.42	5.57	0.08	24.7%	3.5%
15	21	50.7	53.7	29.7	32.7	58.6%	60.9%	30.61	27.74	9.61	4.96	31.4%	24.3%
16	27	53	40.3	26	13.3	49.1%	33.0%	32.04	20.23	5.04	6.93	15.7%	33.5%
17	16	30.5	54	14.5	38	47.5%	70.4%	18.02	27.91	2.02	10.09	11.2%	42.7%
18	16	25.5	48.7	9.5	32.7	37.3%	67.1%	14.91	24.94	1.09	7.76	7.3%	35.8%
19	15	36.1	54	21.1	39	58.4%	72.2%	21.51	27.91	6.51	11.09	30.3%	46.3%
20	17	34.1	49.5	17.1	32.5	50.1%	65.7%	20.27	25.39	3.27	7.11	16.1%	33.0%
21	17	38.1	59.6	21.1	42.6	55.4%	71.5%	22.76	31.05	5.76	11.55	25.3%	45.2%
22	21	35.1	55.4	14.1	34.4	40.2%	62.1%	20.89	28.69	0.11	5.71	0.5%	26.8%
23	20	25.2	58.5	5.2	38.5	20.6%	65.8%	14.72	30.43	5.28	8.07	35.9%	34.3%
24	16	54	50.6	38	34.6	70.4%	68.4%	32.67	26.00	16.67	8.60	51.0%	38.5%
25	13	32.4	47.5	19.4	34.5	59.9%	72.6%	19.21	24.27	6.21	10.23	32.3%	46.4%
26	16	40.4	72.2	24.4	56.2	60.4%	77.8%	24.19	38.11	8.19	18.09	33.9%	58.0%
27	18	39.4	40	21.4	22	54.3%	55.0%	23.57	20.06	5.57	1.94	23.6%	10.3%
28	18	68.3	66.9	50.3	48.9	73.6%	73.1%	41.58	35.14	23.58	13.76	56.7%	48.8%
29	15	48.5	40.3	33.5	25.3	69.1%	62.8%	29.24	20.23	14.24	5.07	48.7%	25.9%
30	22	60.1	54	38.1	32	63.4%	59.3%	36.47	27.91	14.47	4.09	39.7%	21.2%
Average:	17.9	40.2	52.7	22.3	34.8	52.5%	64.7%	24.1	27.2	7.2	8.1	28.1%	33.8%

APPENDIX K. 7.6 CM DEPTH COMPARISON

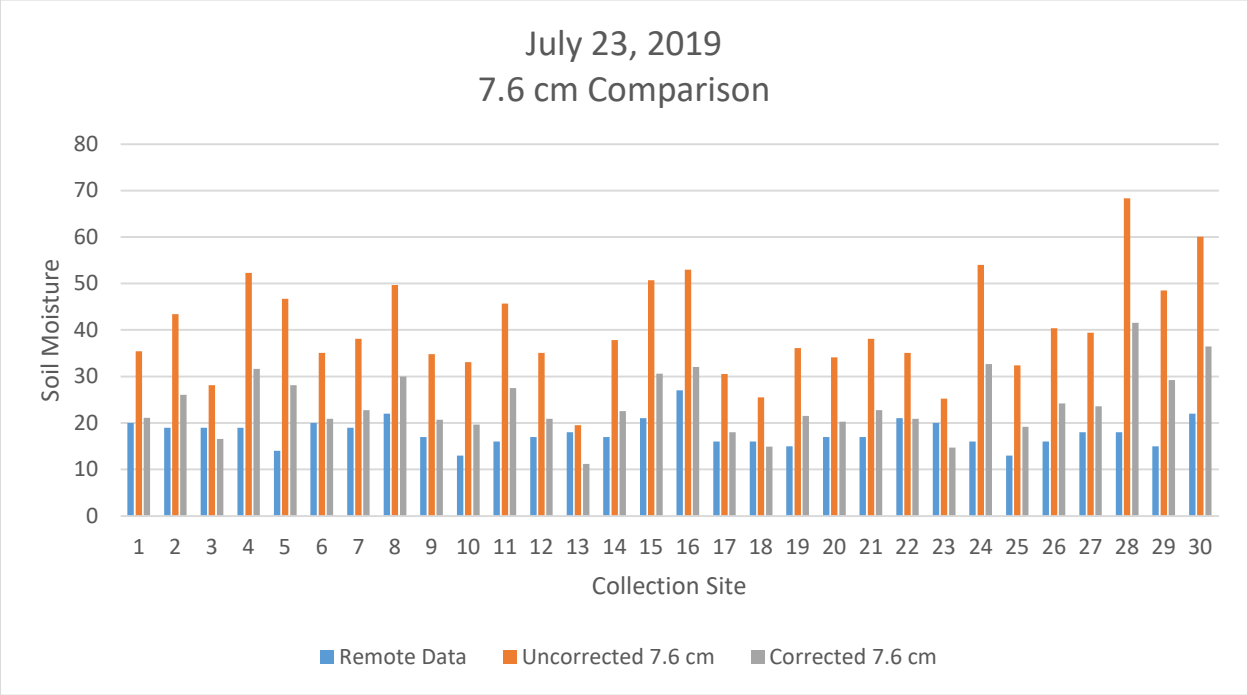

APPENDIX L. 20 CM DEPTH COMPARISON